Anti-inflammatory activity of the rhizomal extract and 4-methoxycinnamyl *p*-coumarate from *Etlingera pavieana* in microglial cells.

MAYUREE POONASRI

A THESIS SUBMITTED IN PARTIAL FULFILLMENT OF
THE REQUIREMENTS FOR THE MASTER DEGREE OF SCIENCE
IN BIOCHEMISTRY
FACULTY OF SCIENCE
BURAPHA UNIVERSITY
2021

ฤทธิ์ต้านการอักเสบของสารสกัดและสาร 4-methoxycinnamyl *p*-coumarate จากเหง้าเร่วหอมในเซลล์ไมโครเกลีย

มยุรีย์ ปูนาศรี

วิทยานิพนธ์นี้เป็นส่วนหนึ่งของการศึกษาตามหลักสูตรวิทยาศาสตรมหาบัณฑิต
สาขาวิชาชีวเคมี
คณะวิทยาศาสตร์ มหาวิทยาลัยบูรพา
2564

Anti-inflammatory activity of the rhizomal extract and 4-methoxycinnamyl *p*-coumarate from *Etlingera pavieana* in microglial cells.

MAYUREE POONASRI

A THESIS SUBMITTED IN PARTIAL FULFILLMENT OF
THE REQUIREMENTS FOR THE MASTER DEGREE OF SCIENCE
IN BIOCHEMISTRY
FACULTY OF SCIENCE
BURAPHA UNIVERSITY
2021

The Thesis of Mayuree Poonasri has been approved by the examining committee to be partial fulfillment of the requirements for the Master Degree of Science in Biochemistry of Burapha University

Advisory Committee

Principal advisor

.....

(Associate Professor Klaokwan Srisook)

Examining Committee

.....

Principal examiner

(Assistant Professor Natthakarn Chiranthanut)

.....

Member

(Associate Professor Klaokwan Srisook)

.....

Member

(Pornpun Aramsangtienchai)

.....

Dean of the Faculty of Science

(Assistant Professor Ekaruth Srisook)

.....

This Thesis has been approved by Graduate School Burapha University to be partial fulfillment of the requirements for the Master Degree of Science in Biochemistry of Burapha University

.....

Dean of Graduate School

(Associate Professor Dr. Nujjaree Chaimongkol)

.....

61910074: MAJOR: BIOCHEMISTRY; M.Sc. (BIOCHEMISTRY)
KEYWORDS: -

MAYUREE POONASRI : ANTI-INFLAMMATORY ACTIVITY OF THE RHIZOMAL EXTRACT AND 4-METHOXYCINNAMYL *P*-COUMARATE FROM *ETLINGERA PAVIEANA* IN MICROGLIAL CELLS.. ADVISORY COMMITTEE: KLAOKWAN SRISOOK, Ph.D. 2021.

-

ACKNOWLEDGEMENTS

-

Mayuree Poonasri

TABLE OF CONTENTS

Page

มหาวิทยาลัยบูรพา
BURAPHA UNIVERSITY

REFERENCES

มหาวิทยาลัยบูรพา
BURAPHA UNIVERSITY

BIOGRAPHY

The Thesis of Mayuree Poonasri has been approved by the examining committee to be partial fulfillment of the requirements for the Master Degree of Science in Biochemistry of Burapha University

Advisory Committee

Principal advisor

..... (Associate Professor Dr. Klaokwan Srisook)

Examining Committee

..... Principal examiner (Assistant Professor Dr. Natthakarn Chiranthanut)

..... Member (Associate Professor Dr. Klaokwan Srisook)

..... Member (Dr. Pornpun Aramsangtienchai)

..... Dean of the Faculty of Science
(Assistant Professor Dr. Ekaruth Srisook)

.....

This Thesis has been approved by the Graduate School Burapha University to be partial fulfillment of the requirements for the Master Degree of Science in Biochemistry of Burapha University

..... Dean of the Graduate School
(Associate Professor Dr. Nujjaree Chaimongkol)

.....

This master thesis has been granted funding support by Graduate School, Burapha University, Fiscal Year 2020

61910074: MAJOR: BIOCHEMISTRY; M.Sc. (BIOCHEMISTRY)
KEYWORDS: ANTI-INFLAMMATORY ACTIVITY/ NITRIC OXIDE/ PROSTAGLANDINS E_2/ TUMOR NECROSIS FACTOR-α/ MICROGLIAL CELLS/ *ETLINGERA PAVIEANA*/ 4-METHOXYCINNAMYL *P*-COUMARATE

MAYUREE POONASRI: ANTI-INFLAMMATORY ACTIVITY OF THE RHIZOMAL EXTRACT AND 4-METHOXYCINNAMYL *P*-COUMARATE FROM *ETLINGERA PAVIEANA* IN MICROGLIAL CELLS. ADVISORY COMMITTEE: KLAOKWAN SRISOOK, Ph.D. 2021.

Etlingera pavieana (Pierre ex Gagnep) R.M. Sm. is a Zingiberaceae plant. The rhizome is widely used as a traditional medicine and a spice. Previous studies have demonstrated that *E. pavieana* rhizomes and 4-methoxycinnamyl *p*-coumarate (MCC) isolated from its rhizomes show anti-inflammatory activity in mouse macrophages and human endothelial cells. Also, MCC has been demonstrated to exhibit *in vivo* anti-inflammatory activity in acute inflammation rat models. Nonetheless, the anti-inflammatory activities of *E. pavieana* rhizome extract and MCC in microglial cells have not yet been demonstrated. Therefore, in the present study, the ethanol extract (EPE) and MCC from *E. pavieana* rhizome were evaluated for their anti-inflammatory activity and the molecular mechanism underlying their anti-inflammatory activity in lipopolysaccharide (LPS)-stimulated BV2 microglial cells. EPE and MCC were assessed for cytotoxicity on microglial cells by the MTT assay, and their non-toxic concentration was used to evaluate the anti-inflammatory activity. Anti-inflammatory activity was evaluated by using the production of nitric oxide (NO), prostaglandins E_2 (PGE_2) and tumor necrosis factor alpha (TNF-α) as indicators. The levels of crucial enzymes and key molecules in the nuclear factor-kappa B (NF-κB) as well as the mitogen activated proteins kinase (MAPKs) signaling pathways were determined by qRT-PCR and Western blot analysis. The results showed that EPE remarkably reduced the production of NO and PGE_2 in a concentration-dependent manner with IC_{50} value of 52.10±1.78 µg/mL and 37.32±6.92 µg/mL, respectively. EPE also decreased the expression of inducible nitric oxide synthase (iNOS) and cyclooxygenase-2 (COX-2) at both mRNA and

protein levels. Furthermore, EPE suppressed NF-κB activation by attenuating the phosphorylation of nuclear factor-kappa B inhibitor alpha (IκBα) and NF-κB p65 subunit. In addition, MCC at non-cytotoxic concentrations considerably reduced both NO and PGE_2 production in a concentration-dependent manner with an IC_{50} value of 3.32±1.13 μM and 13.32±2.18 μM, respectively. Also, MCC significantly suppressed the expression of iNOS and COX-2 at mRNA and protein levels. Additionally, MCC clearly reduced the production of TNF-α in a concentration-dependent manner with an IC_{50} value of 36.01±14.47 μM. Concomitantly, the expression of TNF-α mRNA level was discouraged by MCC. Moreover, MCC inactivated NF-κB signaling by decreasing the phosphorylation of IκBα and the NF-κB p65 subunit. Besides, MCC significantly attenuated the phosphorylation of p38 mitogen-activated kinase (p38 MAPK) and c-Jun N-terminal kinase (JNK). Conversely, the phosphorylation of extracellular signal-regulated kinase (ERK) was significantly increased by MCC. In conclusion, the results suggest that EPE and MCC from *E. pavieana* rhizomes exert an anti-inflammatory activity in LPS-induced BV2 microglial cells. EPE suppressed NO and PGE_2 production via blockade of the NF-κB signaling pathway. MCC also inhibited the production of pro-inflammatory mediators and cytokine through the NF-κB and MAPKs signaling pathways. Accordingly, they might have the potential to be developed as functional food ingredients and dietary supplements for preventing neurodegenerative diseases.

ACKNOWLEDEGEMENTS

There are many people whom I would like to thank for their contributions, both directly and indirectly, to this thesis. Foremost, I would like to express my sincere gratitude to my principal advisor, Associate Professor Dr. Klaokwan Srisook, for giving me the opportunities and providing invaluable guidance throughout the research and writing of this thesis. She has taught me the methodology for carrying out research and how to present the research work as clearly as possible. It was a great fortune to work and study under her guidance.

Besides my advisor, I would like to express my sincere gratitude to Assistant Professor Dr. Natthakarn Chiranthanut for providing microglial cell line for this study, and Assistant Professor Dr. Ekaruth Srisook for kindness in giving me the extraction compound that was used in this study. My sincere thanks also goes to my thesis committee: Assistant Professor Dr. Natthakarn Chiranthanut, Associate Professor Dr. Klaokwan Srisook and Dr. Pornpun Aramsangtienchai for their insightful comments and valuable suggestions on my thesis.

My great appreciation is also given to Biochemistry program, Department of Biochemistry, Faculty of Science and all the lecturer for their encouragement, motivation, and immense knowledge.

This work was partially supported by the Science Innovation Facility, Faculty of Science, Burapha University (SIF-IN-61910074). And, I would like to thank Faculty of Science, Burapha University and the Center of Excellence for Innovation in Chemistry (PERCH-CIC), Commission on Higher Education, Ministry of Education for their financial supports.

Finally, I am sincerely grateful to my family for their love, support, and reliability. Unforgettable, I also special thanks to all of my friends and KS Lab members for their friendship, kindness, help, and suggestions.

Mayuree Poonasri

THE RELEVANCE OF THE RESEARCH WORK TO THAILAND

The main purpose of this study is to evaluate the anti-inflammatory activity of the ethanol extract and 4-methoxycinnamyl *p*-coumarate from *E. pavieana* rhizome and investigate the molecular mechanism underlying the anti-inflammatory effect of 4-methoxycinnamyl *p*-coumarate. This research provides the scientific evidence for used the extract and compound from *E. pavieana* as a new dietary supplement or therapeutic agent for preventing neurodegenerative diseases.

TABLE OF CONTENTS

TABLE OF CONTENTS (CONTINUED)

TABLE OF CONTENTS (CONTINUED)

TABLE OF CONTENTS (CONTINUED)

LIST OF TABLES

LIST OF FIGURES

LIST OF FIGURES (CONTINUED)

LIST OF FIGURES (CONTINUED)

CHAPTER 1
INTRODUCTION

1.1 Statement and significance of the problems

Neurodegenerative diseases are a family of diseases caused by the degeneration of neurons. The common neurodegenerative diseases include Alzheimer's disease, Parkinson's disease and Huntington's disease (Gao & Hong, 2008; Cascione, De Matteis, Leporatti & Rinaldi, 2020). Nowadays, millions of people worldwide combat with neurodegenerative diseases (National Institute of Environmental Health Sciences [NIH], 2021). As of the World Health Organization (WHO) report, neurodegenerative diseases affect around 50 million people worldwide in 2020 and there are nearly 10 million new cases every year. The risk of being affected by a neurodegenerative disease rises considerably with age (Durães, Pinto & Sousa, 2018). According to the Department of Mental Health (2018), the elderly in Thailand are living with dementia more than 800,000 people. There are several causes that lead to loss of function and death of nerve cells, and neuroinflammation is one of the causes leading to these disorders (Block & Hong, 2005; Tansey, McCoy, & Frank-Cannon, 2007; Gao & Hong, 2008; Glass, Saijo, Winner, Marchetto & Gage, 2010).

Neuroinflammation is part of the immune response within the central nervous system (CNS) to harmful stimuli mediated by the production of pro-inflammatory mediators and cytokines such as tumor necrosis factor-α (TNF-α), interleukin-6 (IL-6), interleukin-1 (IL-1), prostaglandin E_2 (PGE_2) and nitric oxide (NO) to promote inflammatory response (Smith, Das, Ray, & Banik, 2012; DiSabato, Quan, & Godbout, 2016). These mediators and cytokines are produced by resident immune cells in CNS, microglial cells. They can be activated by several stimulants such as lipopolysaccharide (LPS) from bacteria, Aβ-peptides and neurotoxin (Voet, Prinz, & van Loo, 2018; Lull & Block, 2010; Amor et al., 2014). However, the excessive and chronic production of pro-inflammatory mediators and cytokines leads to neuronal damage over time and ultimately the death of neuron cells (Han, Harris & Zhang, 2017) resulting in neurodegenerative diseases (Amor, Puentes, Baker & Van Der Valk, 2010). Therefore, the discovery of a potential compound inhibiting the

production of inflammatory mediators in microglia cells may be an alternative treatment for these diseases.

Currently, there is no cure for neurodegenerative disease, the treatment options are focused on symptom relief. The types of drugs available to treat neurodegenerative diseases such as cholinesterase inhibitors and memantine for Alzheimer's disease, and Levo-dopa for Parkinson's disease (Kiaei, 2013; Ali, Schleret, Reilly, Chen, & Abagyan, 2015; Poddar, Chakraborty & Banerjee, 2021). However, the conventional therapies with these drugs may help alleviate some of the symptoms associated with neurodegenerative diseases, but they not on effective disease progression. Also, these drugs can cause several side-effects, the most common include dizziness, nausea, headache, somnolence, vomiting and increased blood pressure (Birks, 2006; Kiaei, 2013; Ali, Schleret, Reilly, Chen, & Abagyan, 2015; Gandhi & Saadabadi, 2020). Thus, there is a need for novel compounds for preventing neurodegenerative diseases with low side effect and medicinal plants that show a variety of biological activities are a good choice.

Etlingera pavieana (Pierre ex Gagnep) R.M. Sm., a plant in the family Zingiberaceae, distributes in the Southeastern of Thailand, especially in Chanthaburi and Trat Provinces. The rhizome is commonly used as an ingredient in noodle soups or curries (Poulsen & Phonsena, 2017), and is also used for the treatment of nausea, flatulence, carminative, diuresis and dyspepsia. Previously, the anti-inflammatory activity of *E. pavieana* rhizome has been reported in LPS-stimulated RAW 264.7 macrophages through suppression of iNOS expression and NO production (Srisook, Palachot, Mankhong, & Srisook, 2017). Also, *E. pavieana* rhizome inhibited intracellular ROS production in endothelial cells (Srisook, Udompong, Sawai, & Thongyen, 2018). Recently, Srisook, Potiprasart, Sarapusit, Park, and Srisook (2020) reported anti-vascular inflammatory effect of *E. pavieana* rhizome on TNF-α-induced human endothelial cells by suppressing the expression of vascular adhesion molecule. In addition, 4-methoxycinnamyl *p*-coumarate (MCC) isolated from rhizomes of *E. pavieana* has been previously shown to inhibit LPS-induced expression of inflammatory mediators via down-regulation of the NF-κB, Akt and AP-1 signaling pathways in LPS-stimulated RAW 264.7 macrophages (Mankhong, Srisook, & Srisook, 2017; Mankhong, Iawsipo, Srisook, & Srisook, 2019). Recently, MCC has

been reported to exhibit anti-vascular inflammatory effects by attenuating TNF-α-stimulated vascular adhesion molecule expression in human endothelial cells (Srisook et al., 2020). Moreover, MCC exhibited in *vivo* anti-inflammatory response in an acute inflammation rat model without any sign of toxicity (Chiranthanut, Lertprasertsuke, Srisook, & Srisook, 2021). However, the anti-inflammatory activities of rhizome extract from *E. pavieana* and MCC compound in microglial cells have never been reported. Thus, the aim of this study is to evaluate the anti-inflammatory activity of ethanol extract and MCC from *E. pavieana* rhizome and to investigate the molecular mechanism underlying their anti-inflammatory effect in microglial cells. The obtained data will be used in the development of *E. pavieana* rhizome and MCC as a dietary supplement or an ingredient in functional food for preventing neurodegenerative diseases.

1.2 Objectives

1. To evaluate anti-inflammatory activity of the extract from *E. pavieana* rhizome and 4-methoxycinnamyl *p*-coumarate in LPS-treated microglial cells.

2. To investigate the molecular mechanism underlying the anti-inflammatory effect of 4-methoxycinnamyl *p*-coumarate in microglial cells.

1.3 Hypotheses

The rhizomal extract from *E. pavieana* and 4-methoxycinnamyl *p*-coumarate exert anti-inflammatory activity in microglial cells. NF-κB and MAPKs signaling pathways might be involved in the anti-inflammatory effect of rhizomal extract from *E. pavieana* and 4-methoxycinnamyl *p*-coumarate in microglial cells.

1.4 Contribution to the knowledge

1. The basic evidence of anti-inflammatory activity and its molecular mechanism of the extract from *E. pavieana* rhizome and 4-methoxycinnamyl *p*-coumarate in microglial cells.

2. Discovery of a compound or extract with potential to be developed as a new dietary supplement or therapeutic agent for preventing neurodegenerative diseases.

1.5 Scope of study

Firstly, the effects of the rhizomal extract from *E. pavieana* and 4-methoxycinnamyl *p*-coumarate on cell viability of microglial cells BV2 were determined by MTT assay. Secondly, the production of NO and PGE_2 in these cells were investigated by Griess reaction and ELISA kit assay, respectively. The expression levels of iNOS and COX-2 proteins and mRNA were consequently evaluated by Western blot analysis and qRT-PCR, respectively. Also, the NF-κB activation was investigated by Western blot analysis. In addition, the effects of MCC on TNF-α production and expression were determined by ELISA kit assay and qRT-PCR, respectively. Finally, the effect of MCC on the phosphorylation of MAPKs was explored by Western blot analysis.

CHAPTER 2
LITERRATURE REVIEWS

2.1 Neuroinflammation

Neuroinflammation is an immune response of innate immune cells in the brain to harmful stimuli such as stressors, injury, infectious agents and neurotoxins within the CNS (DiSabato, Quan, & Godbout, 2016; Milatovic, Zaja-Milatovic, Breyer, Aschner, & Montine, 2017). The function of neuroinflammation is to remove injurious stimuli and repair tissue damage in order to restore homeostasis in the brain, allowing injured neurons to recover (Saavedra-López, Casanova, Cribaro & Barcia, 2016).

Once the brain is stimulated by various harmful stimuli like trauma or infections, immunity cells in the CNS are activated and produce pro-inflammatory mediators such as NO, reactive oxygen species (ROS) and cytokines (Figure 2-1) (Morales, Guzmán-Martínez, Cerda-Troncoso, Farías, & Maccioni, 2014; DiSabato, Quan, & Godbout, 2016). Microglial and astrocyte cells play a crucial role during the neuroinflammation process in the production of those mediators which are released to defend against noxious stimuli. However, if the stimulus remains persistent over time, causing a prolonged inflammatory response and leading to excessive production of mediators, it can lead to neuron damage and the death of neuron cells, which is the origin of several neurodegenerative diseases (Heneka et al., 2015; Chen, Zhang, & Huang, 2016).

2.2 The role of microglia in neuroinflammation

Microglia are the CNS's resident immune cells, representing approximately 12% of the total population of glial cells and being the most abundant mononuclear phagocytes in the CNS (Block, Zecca, & Hong, 2007). The origin of the cells is derived from the bone marrow and migrate into the brain very early in development, where they proliferate and distribute in a non-heterogeneous manner around the CNS (Ginhoux et al., 2010; Bazan, Halabi, Ertel, & Petasis, 2012).

Microglia play critical roles in inflammatory responses and support brain homeostasis and plasticity (Kopitar-Jerala, 2015; Voet, Prinz, & van Loo, 2018). Microglia become activated in response to many stimuli such as amyloid plaques, neurotoxin and infectious agent like LPS from bacteria (Gao et al., 2017). In normal state, microglia are responsible for the phagocytosis of cellular debris occurring from apoptosis and normal cell death, as well as other extracellular debris such as damaged cells, foreign matter and plaques (Lull & Block, 2010). When microglia are stimulated, they are rapidly activated by changing morphology from resting microglia into activated and move towards the site of injury to promote inflammation. Activated microglia release pro-inflammatory elements such as ROS, NO, TNF-α, IL-1β and IL-6 to defense against pathogens (Liu & Hong, 2003). On the other hand, these mediators also drive chronic neuron damage and ultimately the death of neuron cells resulting in various neurodegenerative diseases (Chen, Zhang, & Huang, 2016).

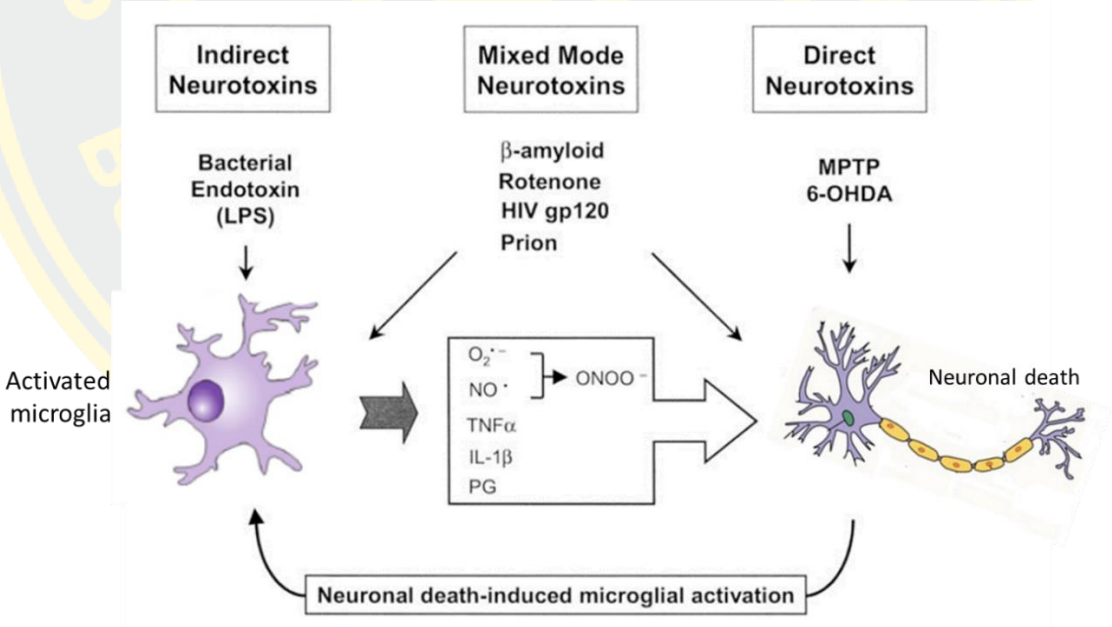

Figure 2-1 Microglia-mediated neuroinflammation by various stimulants (Modified from Gao et al., 2017).

2.3 Pro-inflammatory mediators and cytokines

2.3.1 Nitric oxide and nitric oxide synthase

Nitric oxide (NO) is a free radical signaling molecule that plays a key role in the physiology and the pathophysiology of many human organ systems such as neurotransmitter in the brain system and regulator of vasculature and immune system (Zhou & Zhu, 2009). NO can be synthesized from L-arginine to L-citruline by nitric oxide synthase (NOS) which utilizes oxygen molecule and reduced nicotinamide-adenine-dinucleotide phosphate (NADPH) as co-substrates and also requires (6R-) 5,6,7,8-tetrahydro-L-biopterin (BH_4), flavin adenine dinucleotide (FAD) and flavin mononucleotide (FMN) as cofactors (Figure 2-2) (Förstermann & Sessa, 2011). NOS can be classified into three isotypes including neuronal NOS (nNOS or NOS I), inducible NOS (iNOS or NOS II) and endothelial NOS (eNOS or NOS III). nNOS and eNOS are constitutively expressed and involved in neuronal signaling and vasodilation, respectively. They are stimulated by cellular massive calcium (Ca^{2+}) and calmodulin and produce small quantities of NO. On the other hand, iNOS is an inducible form which produces a large amount of NO when exposure with stimuli (Dagdeviren, 2017).

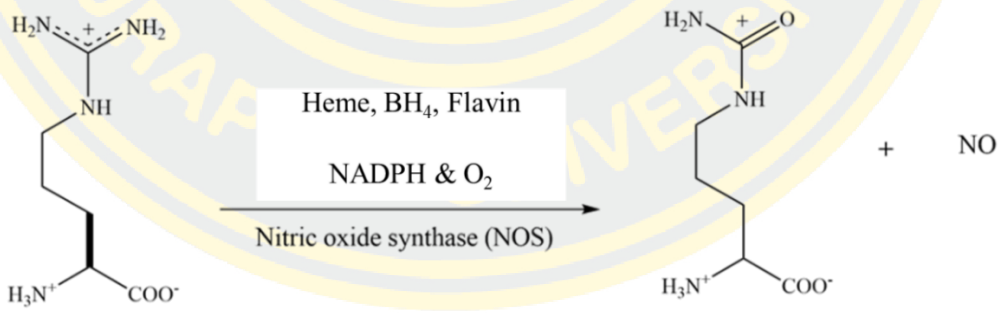

Figure 2-2 NO formation by NOS (Modified from Calabrese et al., 2007)

2.3.2 Prostaglandin E_2 and cyclooxygenase

Prostaglandins (PGs) are a group of lipids derived from arachidonic acid liberated from phospholipids. PGs are synthesized in two-step conversion by the action of cyclooxygenase (COX) (Figure 2-3). They play a critical role in diverse biological activities such as neurons activation, blood pressure and regulation of

immune response. Among prostanoid generated in *vivo* including prostaglandin D_2 (PGD_2), prostaglandin E_2 (PGE_2), prostaglandin $F_{2\alpha}$ ($PGF_{2\alpha}$), prostacyclin (PGI_2) and thromboxane A2 (TxA_2) (Ricciotti & FitzGerald, 2011; Fitzpatrick et al., 2004), PGE_2 is mainly abundant in the body and play an important role in neuroinflammatory response, which are released by neuronal and glial cells in response to inflammatory challenge (Hein & O'Banion, 2009).

Two isozymes of COX have been identified, COX-1 and COX-2. COX-1 is constitutively expressed and produces cytoprotective PGE_2 for lung, kidney, duodenum and kidney. The expression of COX-2 can be induced by many stimuli such as LPS and pro-inflammatory cytokines (Lima, Bastos, Limborço-Filho, Fiebich, & de Oliveira, 2012).

2.3.3 Tumor necrosis factor alpha (TNF-α)

TNF-α is a prominent pro-inflammatory cytokine that regulates inflammatory response in body and brain (Wang, Huang, Chen, Chang, & Kuo, 2010; Neniskyte, Vilalta, & Brown, 2014). It exists in two forms: a membrane-bound protein of 26 kDa and a soluble protein of 17 kDa (Smith, Das, Ray, & Banik, 2012; Wang, Tan, Yu, & Tan, 2015). TNF-α can be produced by a variety of immune cells, with activated microglia being one of the most common sources in the CNS (Kuno et al., 2005; Brás et al., 2020). The production of TNF-α mediates the recruitment, activation and adherence of circulating phagocytic cells and termination of the innate immune response (Ott et al., 2007). Up-regulation of TNF-α plays a role in both neuroprotection and neurodegeneration in the CNS (Wang, Tan, Yu, & Tan, 2015). TNF-α plays a critical role in brain development under normal conditions. In pathological conditions, overactivated microglia release large amounts of TNF-α, causing neuronal damage (Olmos & Lladó, 2014; Wang, Tan, Yu, & Tan, 2015; Brás et al., 2020).

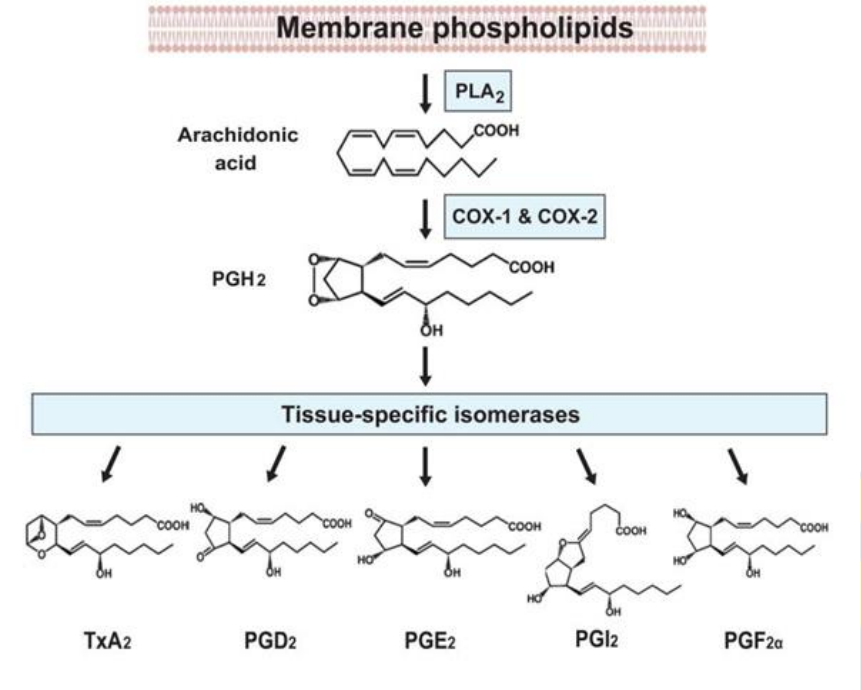

Figure 2-3 Biosynthesis pathway of prostanoids from arachidonic acid (Ricciotti & FitzGerald, 2011).

2.4 Inflammatory signaling pathways

2.4.1 Nuclear factor-kappa B (NF-κB) signaling pathway

NF-κB is a transcription factor that plays a major role in the regulation of genes related with inflammation such as cytokines, chemokines, PGs and NO (Sun, 2011). NF-κB family comprises five subunits, including p65 (RelA), RelB, c-Rel, p50/p105 (NF-κB1), and p52/p100 (NF-κB1) (Hayden & Ghosh, 2008; Dresselhaus & Meffert, 2019). The ubiquitous NF-κB heterodimers found in most cell types are composed of p65 (RelA) and p50 subunits. In normal conditions of cells, NF-κB dimers interact with the inhibitory protein of NF-κB (IκB) to form an NF-κB-IκB complex which remains inactive in the cytoplasm (Hoesel & Schmid, 2013). Nevertheless, in response to cell stimulation, the IkBα is phosphorylated by the activation of IκB kinase complex (IKK). IKK is composed of two catalytically active kinases, including IKKα and IKKβ subunits, and a regulatory protein called NEMO (IKKγ) (Kopitar-Jerala, 2015). Activated IKK phosphorylates IkBα on specific serine

residues, resulting in ubiquitination and proteasomal degradation of IkBα (Dresselhaus & Meffert, 2019). Thus, the free NF-κB dimers translocate into the nucleus and bind to a promotor region of target genes such as pro-inflammatory cytokines and mediators and enhance their transcription (Frakes et al., 2014; Kopitar-Jerala, 2015). The NF-κB activation involves two main signaling pathways, including the canonical and noncanonical pathways, both of which are crucial for controlling immune and inflammatory responses. The canonical pathway's mechanism, NF-κB is activated following IκBα degradation, which is triggered its site-specific phosphorylation by a multi-subunit IκB kinase (IKK) complex. On the other hand, the noncanonical activation does not involve the degradation of IκBα but rather relies on the processing of the NF-κB2 precursor protein p100 (Liu, Zhang, Joo, & Sun, 2017).

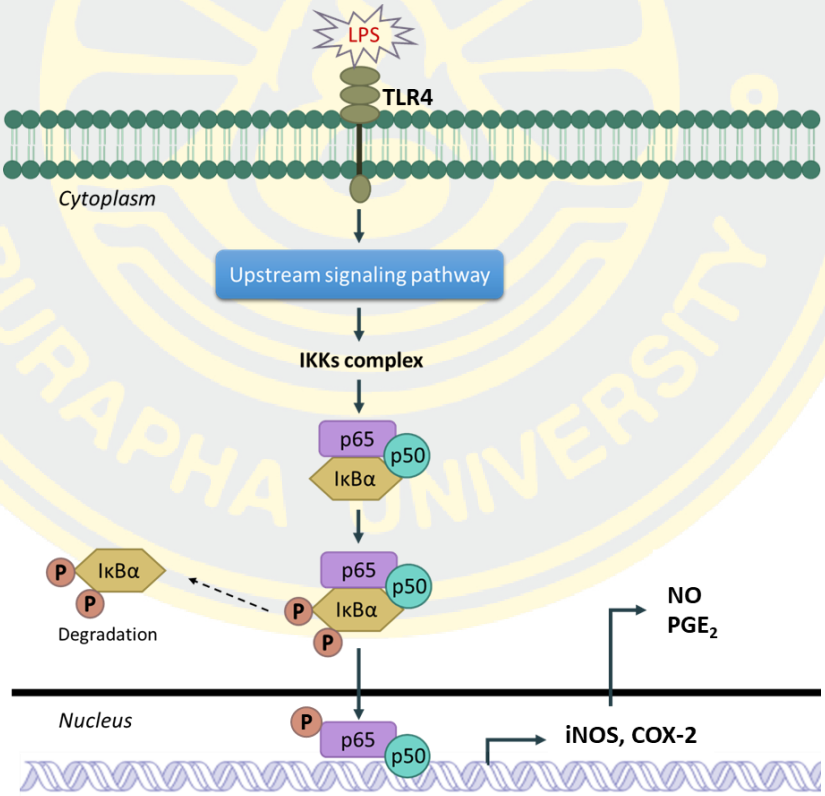

Figure 2-4 Activation of the NF-κB signaling pathways (Modified from Jost & Ruland, 2007; Sun, 2011).

2.4.2 Mitogen activated proteins kinase (MAPKs) signaling pathway

Mitogen-activated protein kinases (MAPKs) are a family of signaling molecules that play an important role in the regulation of cell growth, cell differentiation, cell proliferation, inflammatory responses and cell death (Rose, Force, & Wang, 2010; Kim & Choi, 2010). The major common MAPKs are extracellular signal-regulated kinases (ERK), stress-activated protein kinases (p38), and c-Jun N-terminal kinases (JNK). Signaling transduction from Toll-like receptor (TLR) to MAPKs occurs through the sequential activation of upstream MAP3Ks, MAP2Ks and MAPK (Figure 2-5) resulting in the regulation of a number of cellular activities such as the production of pro-inflammatory cytokines and mediators (Kim & Choi, 2010).

2.4.2.1 Extra-cellular signal-regulated kinases (ERKs)

ERKs consist with ERK1 and ERK2, regulate a large number of cellular and physiological functions, including cell proliferation, cell differentiation, cell death, transcription, cell adhesion and cytokinesis (Grewal, York, & Stork, 1999; Ramos, 2008). To induce cellular processes, ERKs cascade reaction can be activated by a diversity of extracellular substances like hormones, growth factors and cellular stresses. ERKs activation are responsible for stimulating the downstream effectors and can also phosphorylate corresponding protein kinases in cytoplasm, cell membrane, and many transcription factors such as c-Fos, Elk1, p53 and Ets1/2 (Shaul & Seger, 2007; Li et al., 2016).

2.4.2.2 c-Jun N-terminal kinases (JNKs)

JNKs are stress-activated protein kinases containing three isoforms; JNK1, JNK2 and JNK3. JNK1 and JNK2 are ubiquitously expressed while JNK3 is found mostly in the heart, testis, and brain (Rose, Force, & Wang, 2010). JNKs play a role in diverse of biological processes such as cell proliferation, cell differentiation, cell survival, cell apoptosis, and cytokine production. JNKs cascade are crucial in responding to stress and triggering apoptosis in response to diverse stimuli. JNKs pathway are mostly activated in response to inflammatory cytokines and cellular stressors such as oxidant stress, UV radiation, DNA damage and heat shock (Keshet & Seger, 2010).

2.4.2.3 p38 MAPK

Another stress-activated MAPK cascade is that of p38 MAPK which contain four isoforms including p38α, p38β, p38γ and p38δ. They have a similar activation mechanism and substrate specificity. p38α and p38β are ubiquitously expressed, whereas p38γ and p38δ are expressed differently based on tissue type. The activation of p38 occurs via dual phosphorylation by MKK3 and MKK6 which can be induced by various stress factors and inflammatory cytokines (Cuenda & Rousseau, 2007). The p38 play various biological roles such as regulating the proliferation, differentiation, cell cycle regulation, cell growth, cell survival, senescence and apoptosis. It also promotes the expression of pro-inflammatory cytokines and adhesion molecules (VCAM-1), which aids in the immune response (Rose, Force, & Wang, 2010).

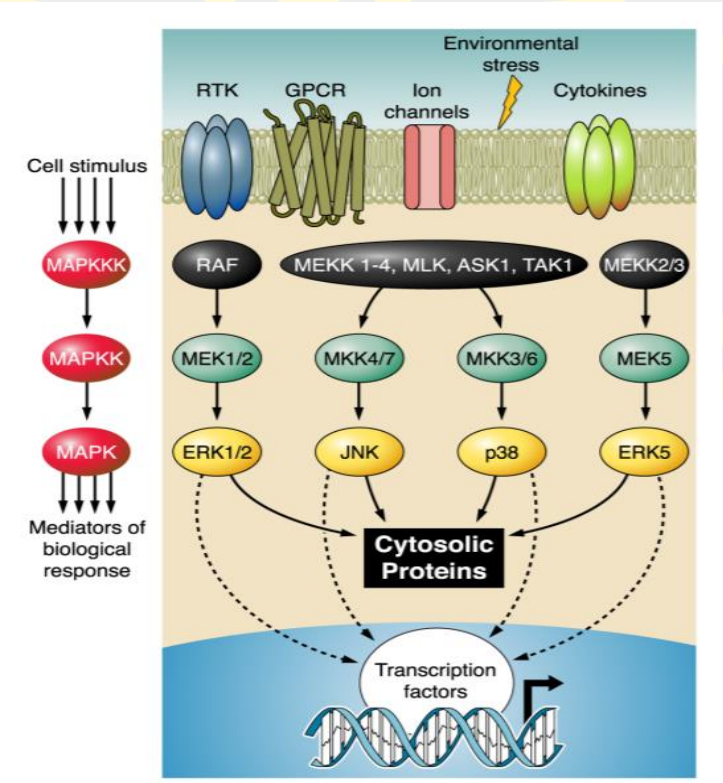

Figure 2-5 Mitogen-activated protein kinases (MAPKs) signaling pathway (Rose, Force, & Wang, 2010).

2.5 Biological activities of *Etlingera pavieana* (Pierre ex Gagnep.) R.M.Sm.

Etlingera pavieana is a plant that belongs to the Zingiberaceae family. *E. pavieana* is common in Lao, Vietnam, Cambodia and southeastern of Thailand, especially in Chanthaburi and Trat Provinces. The local name of *E. pavieana* is "reo hom/rew-hom/raew hawm". The rhizome is used as a spice being an ingredient of noodle soups or boiled with water used as a tonic drink. Medicinal properties are helping the digestive system, anti-flatulent and carminative. In addition, the young shoots of *E. pavieana* also are consumed as a vegetable (Poulsen & Phonsena, 2017).

E. pavieana has been reported to have a variety of biological activities. Tachai and Nuntawong reported six compounds isolated from rhizome of *E. pavieana* including (*E*)-3-(4-methoxyphenyl) prop-2-en-1-amine, (*E*)-1-methoxy-4-(3-methoxyprop-1-enyl) benzene, (*E*)-4-methoxycinamaldehyde, (*E*)-4-methoxycinamic acid, 4-methoxycinnamyl *p*-coumarate and 4-methoxybenzoic acid (Tachai & Nuntawong, 2016). The ethanol extract of *E. pavieana* rhizomes exhibited anti-cancer and anti-oxidant activity (Iawsipo, Srisook, Ponglikitmongkol, Somwang, & Singaed, 2018; Srisook & Srisook, 2011). In addition, Srisook, Udompong, Sawai, and Thongyen reported that *E. pavieana* extracts increased NO bioavailability through inhibiting oxidative stress and activating eNOS expression in human vascular endothelial cells (Srisook, Udompong, Sawai, & Thongyen, 2018). Recently, *E. pavieana* rhizome was reported to exhibit anti-vascular inflammatory effect on TNF-α-stimulated human endothelial cells via suppressing vascular adhesion molecule expression (Srisook et al., 2020). Additionally, the ethyl acetate fraction of *E. pavieana* rhizomes showed an inhibitory effect on LPS-stimulated NO production through iNOS protein and mRNA expression in RAW 264.7 macrophages and four active compounds showing NO inhibitory activity were isolated including, 4-methoxycinnamyl alcohol (MCA), 4-methoxycinnamyl *p*-coumarate (MCC), *trans*-4-methoxycinnamaldehyde (MCD), and *p*-coumaric acid (CM). Among them, MCC showed the best inhibitory activity on LPS-induced NO (Srisook, Palachot, Mankhong, & Srisook, 2017). Moreover, MCC isolated from rhizomes of *E. pavieana* was reported to inhibit LPS-stimulated expression of inflammatory mediators

(Mankhong, Srisook, & Srisook, 2017) by down-regulation of the NF-κB, Akt and AP-1 signaling pathways in LPS-induced RAW 264.7 macrophages (Mankhong, Iawsipo, Srisook, & Srisook, 2019). Also, Srisook and coworkers reported anti-vascular inflammatory effects of MCC in human endothelial cells. The result showed that MCC exhibited anti-vascular inflammatory effects by attenuating TNF-α-stimulated vascular adhesion molecule expression (Srisook et al., 2020). Moreover, MCC exhibited anti-inflammatory response in ethyl phenylpropiolate-induced rat ear edema and carrageenan-induced rat paw edema without any sign of toxicity (Srisook et al., 2021). Besides, MCC was reported the other bioactivities such as anti-bacterial against *Mycobacterium tuberculosis* and anti-cancer activity (Tachai & Nuntawong, 2016).

However, the anti-inflammatory activity of *E. pavieana* in microglial cells has not been reported. Thus, this study aimed to evaluate the anti-inflammatory activity of EPE and MCC in LPS-induced microglial cells.

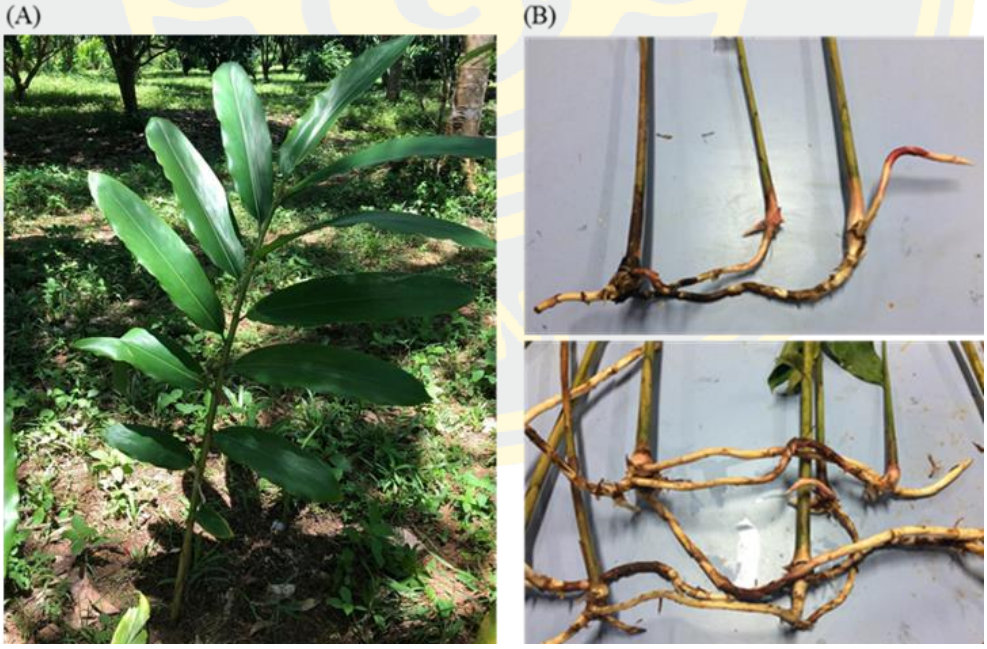

Figure 2-6 *Etlingera pavieana* (Pierre ex Gagnep.) R.M.Sm is composed of the whole plant (A) and the rhizomes (B).

2.6 Techniques involved in this study

2.6.1 Measurement of cell viability by MTT assay

The MTT (3-(4, 5-dimethylthiazolyl-2)-2, 5-diphenyltetrazolium bromide) assay is a colorimetric assay for measuring cell metabolic activity. This method determined cell viability on the basis of the ability of mitochondrial dehydrogenases of living cells in reducing yellow dye of MTT to blue MTT-formazan crystals (Figure 2-7). The formazan formation is representative amount of viable cell mitochondria (Srisook, Palachot, Mongkol, Srisook, & Sarapusit, 2011).

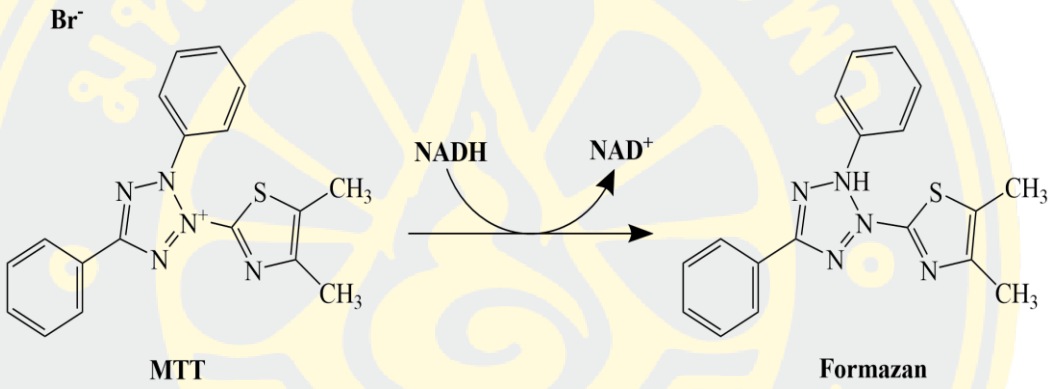

Figure 2-7 The reaction of reducing MTT to formazan product (Modified from Riss et al., 2016).

2.6.2 Measurement of NO production by Griess reaction

The Griess reaction is a method for the indirect determination of NO which oxidized to a stable product nitrite (NO^-_2). The Griess reaction consists of two-steps, which is based on a chemical reaction that uses sulfanilamide and N-(1-napthyl) ethylenediamine (NED) under acidic conditions. NO^-_2 reacts with sulfanilamide to form a diazonium cation, which binds to the NED to form a water-soluble azo compound that absorbs strongly at 540 nm (Figure 2-8) (Tsikas, 2007; Bryan & Grisham, 2007).

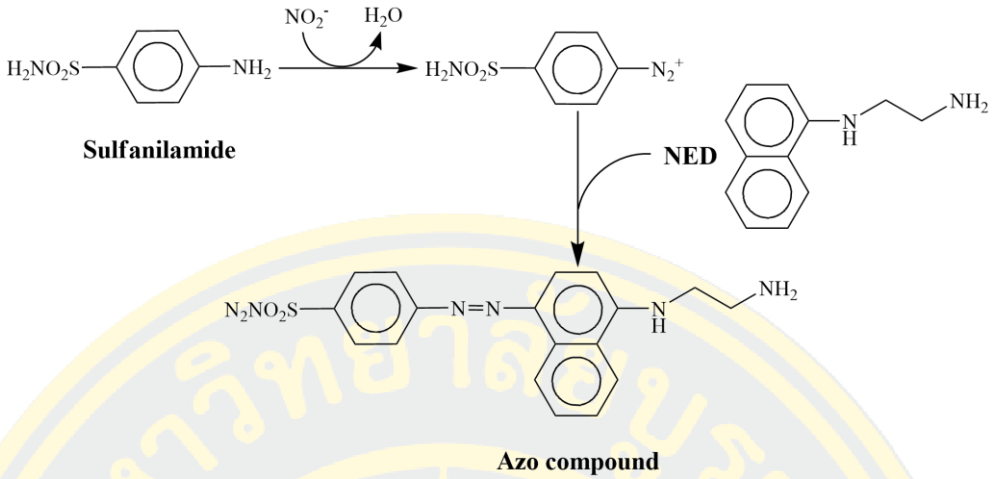

Figure 2-8 Chemical reactions in the measurement of NO_2^- by Griess reagent (Modified from Technical Bulletin protocol, Promega, USA.).

2.6.3 Measurement of PGE_2 and TNF-α production by ELISA Kit assay

ELISA (Enzyme-linked immunosorbent assay) is an immunological technique used for detecting and quantifying the presence of antigens in a given sample.

The competitive ELISA assay technique is used in measurement of PGE_2 production. This assay measures the concentration of an antigen by detection of signal interference. The antibody that specific for a target protein is pre-coated on 96-well plates. The wells are then filled with samples containing the target protein as well as an amount of enzyme-labeled target protein known to be present. The activity of the microplate well-bound enzyme is evaluated after incubation. This indicates that if the antigen amount in the sample is high, the level of antibody-bound enzyme-labeled antigen in the sample is lower, resulting in a lighter color. If it is low, the level of antibody-bound enzyme-labeled antigen in the sample is higher, resulting in a darker color (MBL Life science, 2019).

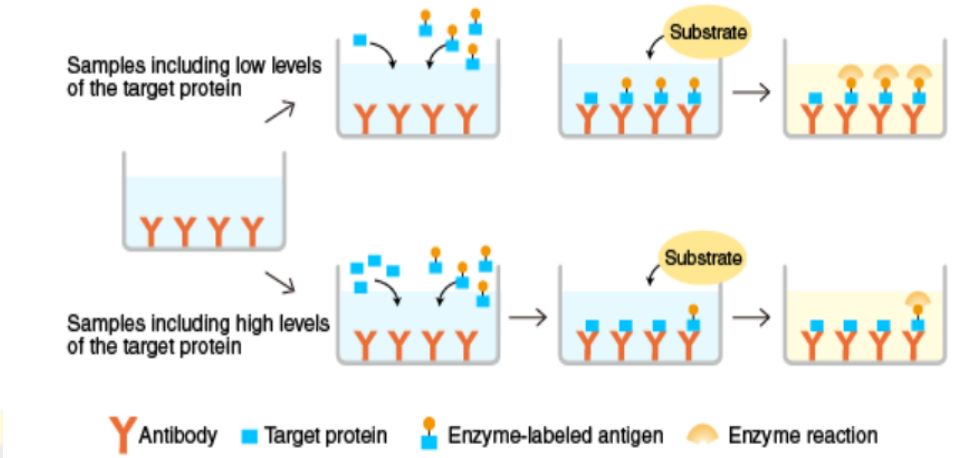

Figure 2-9 An overview of the competitive ELISA assay (MBL Life science, 2019).

The quantitative sandwich ELISA technique is used to quantify amounts of TNF-α. The sandwich ELISA is highly sensitive and the most widely used of the ELISA formats. This assay requires two antibodies specific for different epitopes of the antigen. the target protein antibody is pre-coated on 96-well plates and then incubated with the target protein. Then, in each well, another target protein-specific antibody tagged with an enzyme is added. Unbound antibody-enzyme conjugates are then washed away. Substrate is added, and enzyme converts it to a detectable color (Figure2-10) (Gan & Patel, 2013).

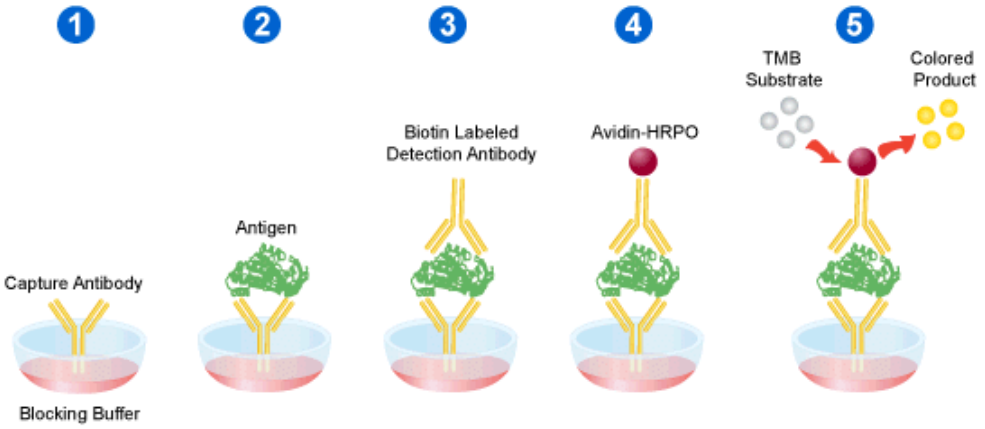

Figure 2-10 An overview of the sandwich ELISA assay (Pomary, 2016).

2.6.4 Western blot analysis for protein expression

Western blotting (protein blotting or immunoblotting) is a sensitive and rapid method for detecting and analyzing proteins. The method is based on the principle of immunochromatography. In this assay, the proteins are applied to gel electrophoresis for separation according to their molecular weight. Then, the separating proteins are transferred from the gel into membrane by electrophoresis. After that, non-protein binding regions on the membrane are blocked to avoid non-specific antibody binding. Consequently, the membrane is incubated with a primary antibody that specifically binds to the interested protein. Unbound antibodies are washed away and a secondary antibody conjugated to an enzyme (Figure 2-11), a fluorophore or an isotope is used to detect the target protein and visualized by a chemiluminescent or chromogenic method. (Mahmood & Yang, 2012).

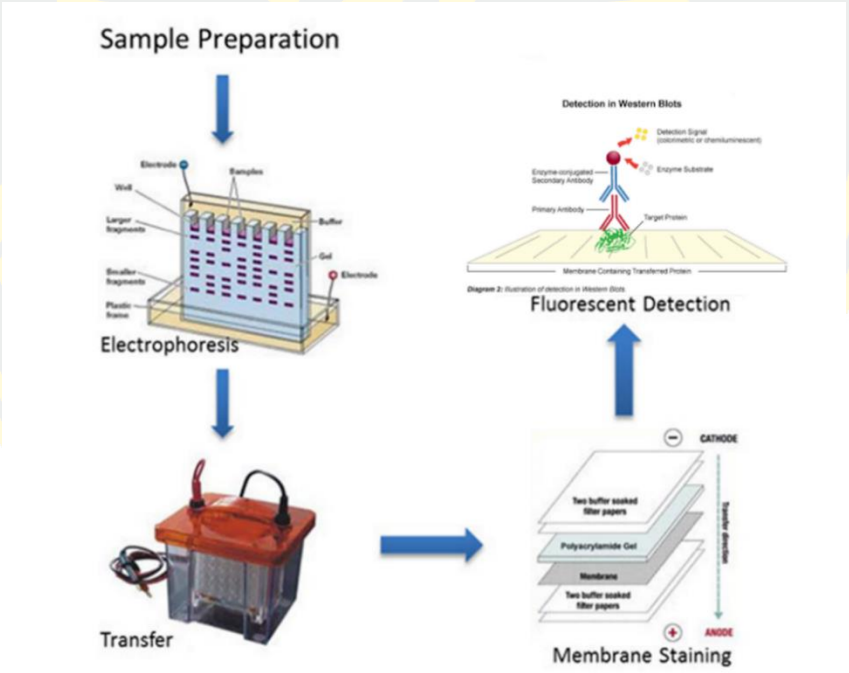

Figure 2-11 Western blot analysis technique (Biology Blog, 2016).

2.6.5 Real time qRT-PCR for mRNA expression

The real-time quantitative reverse transcription-polymerase chain reaction (Real time qRT-PCR) is a PCR-based method that can amplify and detect changes in

amplicon concentration at the same time. During PCR amplification, real-time qRT-PCR captures data by exploiting fluorescence signals emitted by either specific probes or DNA binding dyes. In this technique, RNA transcripts are measured by first reverse transcribing them into cDNA and then performing real-time PCR. DNA is amplified in three phases, similar to standard PCR, including denaturation, annealing, and elongation (Bustin & Mueller, 2005). However, fluorescent labeling allows for data gathering while the PCR continues in real time qRT-PCR. Because of the variety of methodologies and chemistries available, this technology has numerous advantages.

SYBR Green I dye is a fluorescent DNA binding dye that binds to double-stranded DNA's minor groove. When DNA-bound SYBR Green dye is excited, it produces a much stronger fluorescence signal than unbound dye (Figure 2-12). A horizontal baseline is detected in the early PCR cycles. If the target was present in the sample, there will be enough cumulative PCR product produced at some time to allow the amplification signal to be seen (Figure 2-13).

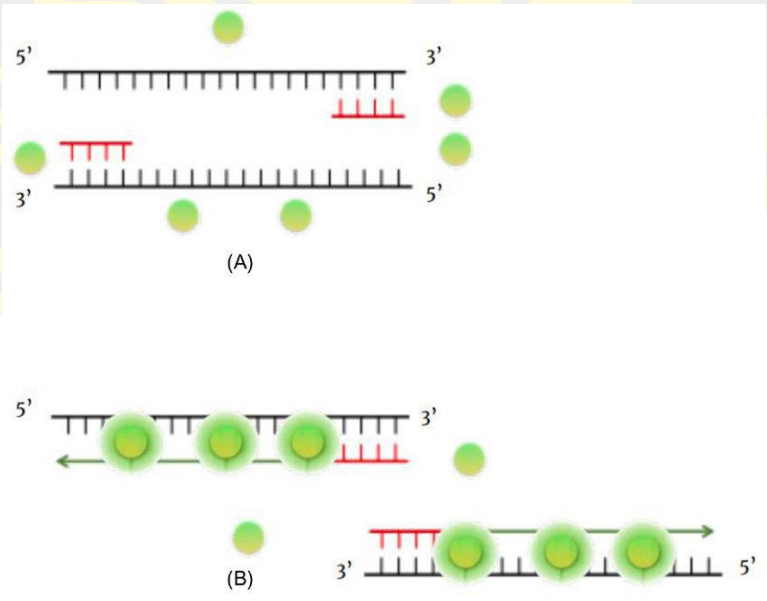

Figure 2-12 The action of SYBR Green I dye. (A) Once DNA is denatured, SYBR Green I Dye floats free and emits low fluorescence. (B) SYBR Green Dye binds to the double-stranded product and emits fluoresces (Basic Science Methods for Clinical Researchers, 2017).

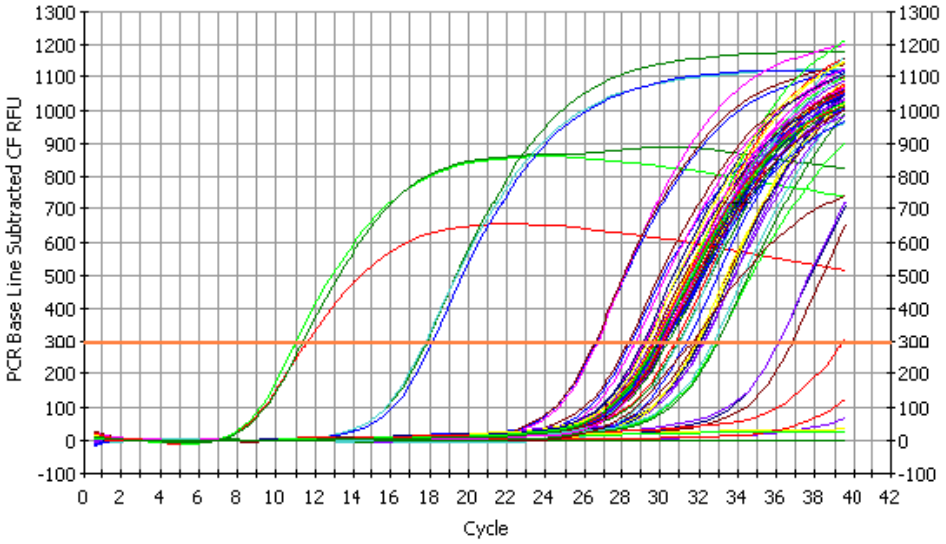

Figure 2-13 Real-time qRT-PCR amplification signal (Daniels, 2012).

CHAPTER 3

RESEARCH METHODOLOGY

An overview of the experiment

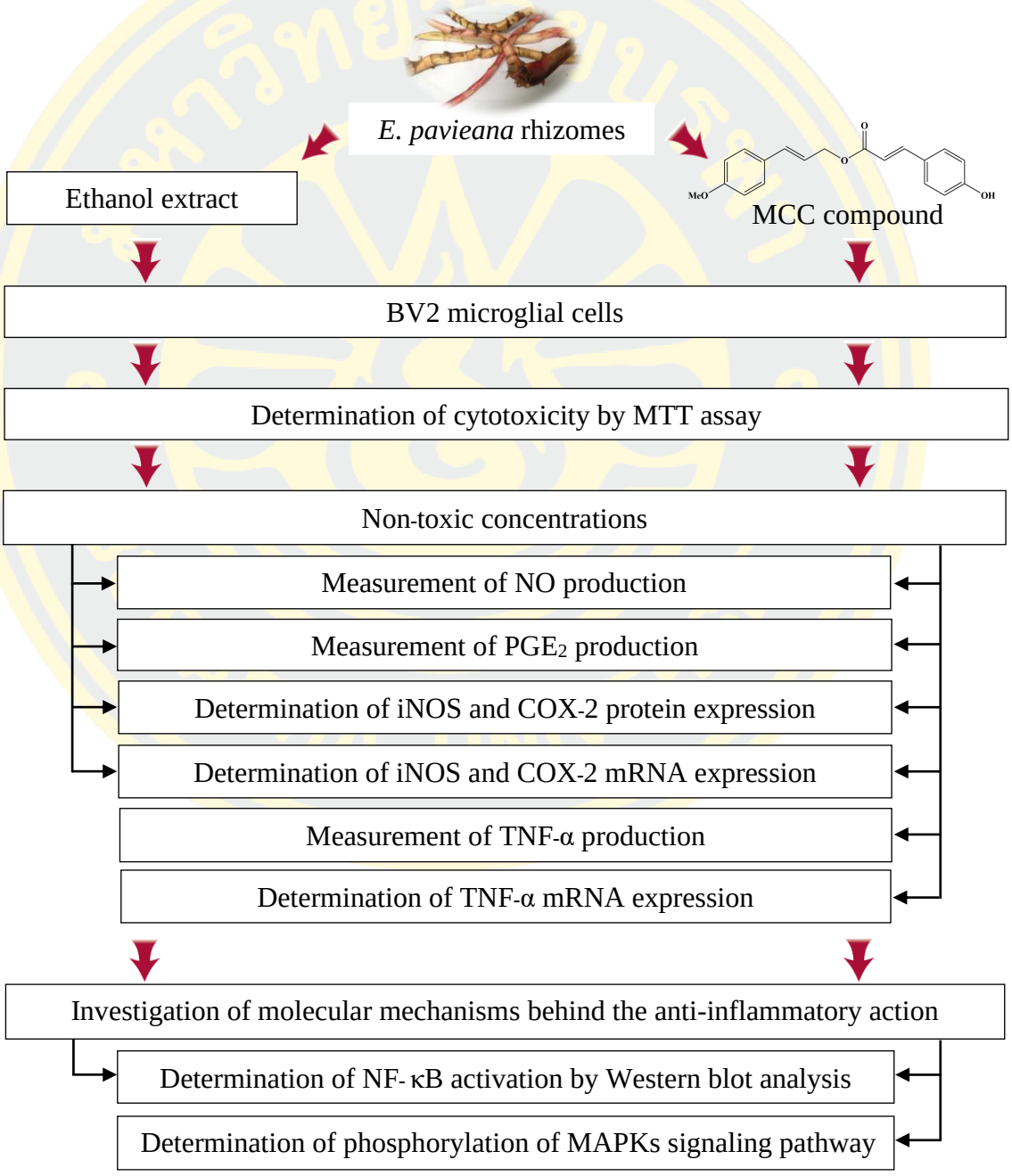

3.1 Materials and equipments

3.1.1 Chemicals

1. 1,2-Di-(dimethylamino) ethane (TEMED) (Calbiochem, USA.)
2. 2-Mercaptoethanol (Sigma-Aldrich, USA.)
3. 2-Propanol (Merck, Germany)
4. 2x iTaq Universal SYBR® Green Supermix (Bio-Rad, USA.)
5. 3-(4,5-Dimethylthiazol-2-yl)-2,5-Diphenyltetrazolium Bromide, MTT (Invitrogen™, USA)
6. 5x iScript Reverse Transcription Supermix for RT-qPCR (Bio-Rad, USA.)
7. Bovine Serum Albumin Standard (Thermo Scientific, USA.)
8. AccuProtein Chroma (Enzmart Biotech, Thailand)
9. Aminoguanidine bicarbonate (Sigma, USA.)
10. Ammonium persulfate (APS) (Plusone, Sweden)
11. Anti-mouse IgG, HRP-linked Antibody (Cat. No. #7076, Cell Signaling Technology, USA.)
12. Anti-rabbit IgG, HRP-linked Antibody (Cat. No. #7074, Cell Signaling Technology, USA.)
13. Autex Manual X-Ray Developer (CPAC Imaging, Thailand)
14. Autex Manual X-Ray Fixer (CPAC Imaging, Thailand)
15. BAY 11-7082 (Merck, USA.)
16. Bis (N,N'-Methylene-bis-acrylamide) (Bio-Rad, USA.)
17. Bovine serum albumin, BSA (Merck, USA.)
18. CL-XPosure™ Film (Thermo Scientific, USA.)
19. COX-2 forward primer 5’-TGATCGAAGACTACGTGCAACACC-3’ (Sigma, USA.)
20. COX-2 reverse primer 5’-TTCAATGTTGAAGGTGTCGGGCAG-3’ (Sigma, USA.)
21. D (+)-glucose (Merck, Germany)
22. Di-Sodium hydrogen phosphate, Na_2HPO_4 (Carlo Erba, Germany)
23. Dimethyl sulfoxide, DMSO (MP biomedical, France)
24. DL-1,4- Dithiothreitol (DTT) (Acros Organic, USA.)

25. Dulbecco's modified Eagle medium with phenol red (Gibco, USA.)
26. Dulbecco's modified Eagle medium without phenol red (Sigma Aldrich, USA.)
27. EF-2 forward primer 5'-CTGAAGCGGCTGGCTAAGTCTGA-3' (Sigma, USA.)
28. EF-2 reverse primer 5'-GGGTCAGATTTCTTGATGGGGATG-3' (Sigma, USA.)
29. ERK1 Antibody (K-23) (Cat. No. sc-94, Santa Cruz Biotechnology, USA.)
30. Ethylene glycol-bis (2-aminorthylether)-N,N,N',N'-tetraacetic acid, EGTA (Sigma, USA.)
31. Absolute ethanol (Merck, Germany)
32. Fetal bovine serum, FBS (Gibco, USA.)
33. GAPDH (14C10) Rabbit mAb (Cat. No. #2118, Cell signaling technology, USA.)
34. Glycine (Bio-Rad, USA.)
35. Halt™ Phosphatase inhibitor cocktail (Thermo Scientific, USA.)
36. Halt™ Protease inhibitor cocktail (Thermo Scientific, USA.)
37. Indomethacin (Sigma, USA.)
38. iNOS forward primer 5'-GCACAGCACAGGAAATGTTTCAGCAC -3' (Sigma, USA.)
39. iNOS reverse primer 5'-AGCCAGCATACCGGATGAGC-3' (Sigma, USA.)
40. IκBα (112B2) Mouse mAb (Carboxy-terminal Antigen) (Cat. No. #9247, Cell signaling technology, USA.)
41. Lipopolysaccharide, LPS from Escherichia coli 0111: B4 (Sigma, USA.)
42. Methanol, ACS Grade (Honeywell Burdick&Jackson, South Korea)
43. Mouse TNF-α Quantikine® ELISA kit (R&D System, USA.)
44. N-(1-naphthyl)-ethylenediamine dihydrochoride (Sigma Aldrich, USA.)
45. Nonidet P-40 (Bio basic inc., Canada)

46. NucleoSpin® RNA (Macherey-nagel. Germany)
47. p38α Antibody (C-20) (Cat. No. sc-535, Santa Cruz Biotechnology, USA.)
48. Penicillin/Streptomycin (Gibco-invitrogen, USA.)
49. Phospho-IκBα (Ser32/36) (5A5) Mouse mAb (Cat. No. #9246, Cell signaling technology, USA.)
50. Phospho-NF-κB p65 (Ser536) (93H1) Rabbit mAb (Cat. No. #3033, Cell signaling technology, USA.)
51. Phospho-p38 MAPK (Thr180/Tyr182) (D3F9) XP® Rabbit mAb (Cat. No. #4511, Cell signaling technology, USA.)
52. Phospho-p44/42 MAPK (Erk1/2) (Thr202/Tyr204) Antibody (Cat. No. #9101, Cell signaling technology, USA.)
53. Phospho-SAPK/JNK (Thr183/Tyr185) Antibody (Cat. No. #9251, Cell signaling technology, USA.)
54. Phosphoric acid (Merck, Germany)
55. Polyoxyethylene-20 (Tween-20) (Bio Basic inc., Canada)
56. Potassium chloride, KCl (Carlo Erba, Germany)
57. Potassium dihydrogen orthophosphate, KH_2PO_4 (BDH Laboratory, UK)
58. Precision Plus Protein™ All Blue Standards (Bio-Rad, USA.)
59. Prostaglandin E_2 Enzyme Immunoassay Kit (Arbor AssayTM, USA.)
60. Protein Assay Dye Reagent Concentrate (Bio-Rad, USA.)
61. Purified Mouse Anti-COX-2 (Cat. No. 610203, BD Biosciences, USA.)
62. Purified Mouse Anti-iNOS/NOS Type II (Cat. No. 610329, BD Biosciences, USA.)
63. Restore™ Plus Western Blot Stripping Buffer (Thermo Scientific, USA.)
64. SAPK/JNK Antibody (Cat. No. #9252, Cell signaling technology, USA.)
65. Skim milk powder (Sigma-Aldrich, USA.)
66. Sodium bicarbonate, $NaHCO_3$ (Sigma, USA.)

67. Sodium chloride, NaCl (Sigma-Aldrich, USA.)
68. Sodium dodecyl sulfate, SDS (Bio-Rad, Japan)
69. Sodium nitrite, $NaNO_2$ (Sigma, USA.)
70. Sterile distilled water (A.N.B. Laboratory, Thailand)
71. Sulfanilamide (Sigma-Aldrich, USA.)
72. SuperSignal® West Pico Chemiluminescent Substrate (Sigma-Aldrich, USA.)
73. TNF-α forward primer 5'-CCCTCACACTCACAAACCACCA-3' (Intergrated DNA Technologies, USA.)
74. TNF-α reverse primer 5'-TGAGGAGCACGTAGTCGGGG-3' (Intergrated DNA Technologies, USA.)
75. Immobilon-P PVDF Membrane, 0.45 µm pore size (Millipore, Germany)
76. Tris (hydroxymethyl) amino methane (Bio-Rad, USA.)
77. Thypan Blue Stain (Gibco, USA.)
78. UltraPure™ Acrylamide (Invitrogen, USA.)

3.1.2 Equipments

1. Centrifuge (K240R, Centurion Scientific, UK)
2. Centrifuge (Z326K, Hermle Labortechnik, Germany)
3. CFX96 Touch™ Real-time PCR (Bio-Rad, USA.)
4. CO_2 incubator (CB210, Binder, Germany)
5. Digital Dry Bath (D1100, Labnet, USA.)
6. Digital Water bath (WB-22, WiseBath, South Korea)
7. Electrophoresis chamber (Mini PROTEIN® Tetra System, Bio-Rad, USA.)
8. Hematometer Improved Neubauer 0.0025 mm2 (Blau Brand, Germany)
9. Hypercassette™ (Amersham Bioscience, USA.)
10. Inverted microscope (Olympus IX70, Japan)
11. Laminar flow class II (NU-440, Nuairre, USA.)
12. Medical X-ray Cassette (Kodak, USA.)
13. Microplate reader (Versamax, molecular Devices, Tunable, USA.)

14. NanoDrop™ One Microvolume UV-Vis Spectrophotometer (Thermo Scientific, USA.)
15. Power supply (PAC300, Bio-Rad, USA.)
16. TE 22 mini tank transfer unit (Amersham Bioscience, USA.)
17. Vortex (Velp Scientification, Italy)

3.2 Methods

3.2.1 Extract and compound preparation

The preparation of ethanol extract of *E. pavieana* (EPE) was performed as described by Srisook et al. (2017). In a brief, *E. pavieana* rhizome was extracted with 95% ethanol. Then extract was filtered under pressure and evaporated by a rotary evaporator, respectively.

The active compound from *E. pavieana* rhizome, 4-methoxycinnamyl p-coumarate (MCC) was provided by Assist. Prof. Dr. Ekaruth Srisook from the Department of Chemistry, Faculty of Science, Burapha University. The chemical structure of MCC is shown in figure 3-1.

EPE and MCC were dissolved in DMSO before being filtered through a 0.2 µm nylon syringe filter. Then, EPE and MCC solutions were aliquoted into a 1.5 mL tube and kept in a refrigerator at -20 ˚C.

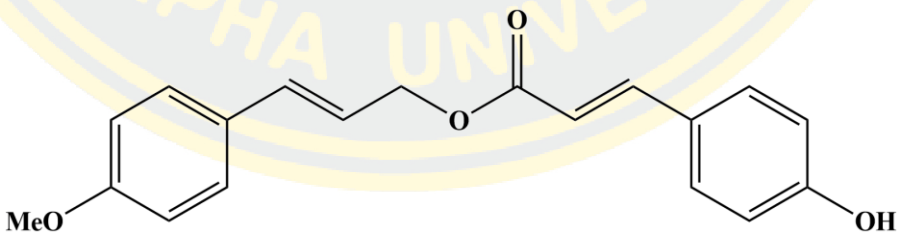

Figure 3-1 The chemical structure of 4-methoxycinnamyl p-coumarate (MCC)

3.2.2 Cell culture

BV2, a murine microglial cell line, was obtained from the Interlab Cell Line Collection (ICLC), which was kindly provided by Assist. Prof. Dr. Natthakarn Chiranthanut from the Department of Pharmacology, Faculty of Medicine, Chiang

Mai University. Cells were cultured in DMEM containing 100 U/ml of penicillin, 100 µg/ml of streptomycin, and 10% heat-inactivated FBS in a humidified containing 5% CO_2 air at 37°C. The cells were subcultured by scraping.

3.2.3 Determination of cell viability by MTT assay

This method was performed as described by Srisook et al. (2011). In a brief, BV2 microglial cells were subcultured into a 24-well plate in a number of 1.5×10^5 cells/well, and incubated at 37 °C for 18-20 h. Then, cells were treated with 500 µL of fresh DMEM containing EPE at various concentrations of 6.25-200 µg/mL or MCC at different concentration of 6.25-200 µM for 24 h. Next, the cultured media was sucked out before adding 500 µL of fresh DMEM containing MTT (0.1 mg/mL) to each well and incubating them further for 2 h. After removing the cultured media, 500 µL of DMSO was used to dissolve formazan crystals in each well, before transferring 200 µL of formazan solution to a 96-well microplate. The absorbance of solution in each well was then measured at 550 nm with a microplate reader. The experiment was replicated at least 3 times with triplicate samples. The percentage of cell viability can be calculated from the equation shown below:

$$\%\text{Cell viability} = \left(\frac{\text{Absorbance of treated well}}{\text{Absorbance of control well}}\right) \times 100$$

3.2.4 Determination of NO, PGE_2 and TNF-α production in BV2 microglial cells

3.2.4.1 Measurement of NO production by Griess reaction

BV2 microglial cells were subcultured into a 24-well plate in a number of 1.5×10^5 cells/well before incubating at 37 ˚C for 18-20 h. The cells were then pre-treated with phenol red-free DMEM containing EPE at the concentrations of 25-100 µg/mL or MCC at the concentrations of 6.25-25 µM or 50 µM of aminoguanidine (a positive control) for 1 h before stimulating with LPS (1 µg/mL) for 24 h. The cultured media in each well was collected and then centrifuged at 13,700 g for 5 min at 4 ˚C. After that, 100 µL of cultured media supernatant was mixed with 100 µL of Griess solution [0.1% (w/v) N-(1-naphathyl)-ethylene diamine dihydrocholide, 1% (w/v) sulfanilamide and 5% (v/v) phosphoric acid] in a 96-well microplate. The absorbance

was measured at 546 nm by a microplate reader. The nitrite concentration was evaluated from the standard curve of sodium nitrite at 3.12-50 µM (Srisook et al., 2015). The percentage of production and inhibition can be calculated with the equation below.

$$\%\text{Production of NO} = \left(\frac{\text{Nitrite concentration of treated well}}{\text{Nitrite concentration of LPS well}} \right) \times 100$$

$$\%\text{Inhibition of NO} = 100 - \left(\frac{\text{Nitrite concentration of treated well}}{\text{Nitrite concentration of LPS well}} \right) \times 100$$

3.2.4.2 Measurement of PGE_2 production by ELISA

A Prostaglandin E_2 Enzyme Immunoassay Kit (Arbor Assay™, USA) was used to determine the quantity of PGE_2 in the cultured media. BV2 microglial cells were subcultured into a 24-well plate in a number of 1.5×10^5 cells/well before incubating at 37 ˚C for 18-20 h. Then, cells were pre-treated with fresh DMEM containing EPE at the concentrations of 25-100 µg/mL or MCC at the concentrations of 6.25-25 µM or 1µM of indomethacin (a positive control) for 1 h before stimulating with LPS (1 µg/mL) for 24 h. Next, the cultured media was collected and centrifuged at 13,700 g for 5 min at 4 ˚C. After that, the quantity of PGE_2 in the supernatant was assessed according to the manufacturer's instructions. In a brief, 10 µL of samples were diluted with 190 µL of Assay buffer, and 50 µL of diluted samples or PGE_2 standards were pipetted into each well of 96-wells coated with goat anti-mouse IgG (provided by the manufacturer). Then, 25 µL of DetectX® Prostaglandin E_2 conjugate was pipetted into each well, followed by adding 25 µL of DetectX® Prostaglandin E_2 antibody, and incubated with shaking at room temperature for 2 h. Next, the solution was aspirated and rinsed each well four times with 300 µL of Wash buffer. After that, 100 µL of substrate TMB was pipetted into each well before incubating without shaking for 30 min at room temperature. At last, 50 µL of stop solution was pipetted into each well before measuring the absorbance at 450 nm with a microplate reader. The quantity of PGE_2 was calculated using a standard curve with known PGE_2 concentrations of 15.625-1000 pg/mL. The experiment was replicated at least 3 times

with duplicate samples. The percentage of production and inhibition can be calculated with the equation below.

$$\%\text{Production of } PGE_2 = \left(\frac{PGE_2 \text{ concentration of treated well}}{PGE_2 \text{ concentration of LPS well}} \right) \times 100$$

$$\%\text{Inhibition of } PGE_2 = 100 - \left(\frac{PGE_2 \text{ concentration of treated well}}{PGE_2 \text{ concentration of LPS well}} \right) \times 100$$

3.2.4.3 Measurement of TNF-α production by ELISA

A mouse TNF-α Quantikine® ELISA kit (R&D System, USA.) was used to assessed the quantity of TNF-α in cultured media. BV2 microglial cells were subcultured into a 24-well plate (1.5×10^5 cells/well) before incubating at 37 ˚C for 18-20 h. Then, cells were pre-treated with fresh DMEM containing MCC at the concentrations of 6.25-25 µM for 1 h before being LPS stimulated. After stimulation for 24 h, the cultured media was collected, followed by centrifugation for 5 min at 13,700 g 4 ˚C. The quantity of TNF-α in the cultured media supernatant was assessed according to the manufacturer's instructions. Briefly, the samples were diluted with Calibrator Diluent RD5K (dilution factor 1:19). Then, 50 µL of diluted samples were mixed with 50 µL of assay diluent RD1-63 in the 96-well coated with monoclonal antibody specific for mouse TNF-α before incubating at room temperature for 2 h. Next, the solution was discarded and rinsed with 400 µL of Wash buffer for each well for 5 times. After that, 100 µL of mouse TNF-α conjugate was pipetted to each well and incubated for 2 h at room temperature, before washing again 4 times. Then, 100 µL of substrate solution was pipetted into each well, followed by incubation for 30 min at room temperature (protect from light). Finally, 100 µL of stop solution was pipetted to each well before measuring the absorbance with a microplate reader set at 450 nm and 540 or 570 nm. The quantity of TNF-α was calculated using a standard curve with known with known concentrations of TNF-α of 10.9-1400 pg/mL. The experiment was replicated at least 3 times with duplicate samples. The percentage of production and inhibition can be calculated with the equation below.

$$\%\text{Production of TNF-}\alpha = \left(\frac{\text{TNF-}\alpha \text{ concentration of treated well}}{\text{TNF-}\alpha \text{ concentration of LPS well}} \right) \times 100$$

$$\%\text{Inhibition of TNF-}\alpha = 100 - \left(\frac{\text{TNF-}\alpha \text{ concentration of treated well}}{\text{TNF-}\alpha \text{ concentration of LPS well}} \right) \times 100$$

3.2.5 Determination of iNOS and COX-2 expression in LPS-induced BV2 microglial cells

3.2.5.1 Preparation of whole cell protein extract

Protein preparation was performed as described by Mankhong (2018). BV2 microglial cells were subcultured into 60-mm plate in a number of 1×10^6 cells/plate before incubating at 37 ˚C for 18-20 h. The cells were pre-treated with fresh DMEM containing EPE at the concentrations of 25-100 µg/mL or MCC at the concentrations of 6.25-25 µM for 1 h before stimulating with LPS (1 µg/mL) for 24 h. Then, the cultured media was discarded and rinsed with cold PBS. Next, cells were lysed and scraped on ice with cold RIPA protein lysis buffer [150 mM Tris-HCL (pH 7.4), 150 mM NaCl, 5 mM EGTA, 0.1% (v/v) SDS, 1% (v/v) Nonidet P-40, 1% (v/v) sodium deoxycholate] containing 1x protease inhibitor cocktail and 1 mM DTT. The cell lysates were centrifuged at 13,700 g for 10 min at 4 ˚C, and supernatant was collected into a new microcentrifuge tube. After that, the protein amount in the supernatant were evaluated using the Bradford protein assay.

3.2.5.2 Determination of protein concentration by Bradford protein assay

Protein concentrations were assessed by Bio-Rad protein assay according to the manufacturer's instructions. Briefly, 2µL of protein and 8 µL of sterile water were mixed into the 96-well plate and 200 µL of 1x Bio-Rad Protein Assay Dye Reagent Concentrate (freshly diluted with distilled water) was added. After shaking for 5 min at room temperature, absorbance was measured at 595 nm by a microplate reader. The protein concentration was calculated from a standard curve of bovine serum albumin (BSA) dissolved in sterile water (0.5-6.0 µg).

3.2.5.3 Western blot analysis

This method was described by Mankhong (2018). Brifly, protein extract was mixed with 6x protein loading buffer [124 mM Tris-HCl (pH 6.8), 5% (v/v) β-mercaptoethanol, 10% (v/v) glycerol, 4% (w/v) SDS and 0.01% (w/v) bromophenol blue] (5:1). Then, the protein mixtures were heated in a digital dry bath at 100˚C for 5 min and spun down before subjection to 10% sodium dodecyl sulplate-polyacrylamide electrophoresis (SDS-PAGE) and electrophoresed under a constant voltage of 80 V for 1.30 h with Tris-glycine running buffer [0.192 M glycine, 0.025 M Tris, 0.1% (w/v) SDS]. After that, the separated protein was transferred to a polyvinylidene fluoride (PVDF) membrane using a protein transfer tank under a constant voltage of 25 V at 4 ˚C for overnight.

The membrane was incubated with shaking for 1 h at room temperature with blocking solution (5% (w/v) skim milk dissolved in TBS-T buffer [10 mM Tris-HCl pH 7.5, 100 mM NaCl and 1% Tween 20]) before incubating with specific primary antibodies according to the conditions shown in the table 3-1.

Table 3-1 The conditions for incubation of iNOS, COX-2 and GAPDH primary antibodies

Proteins	Fold of dilution	Dissolvent	Time	Temperature
iNOS	1:1,000	0.5% (w/v) BSA in PBS, 0.05% (v/v) Tween® 20	1 h	Room temp.
COX-2	1:500			
GAPDH	1:1,000	5% (w/v) BSA, 1x TBS, 0.1% Tween® 20		

After incubation time, the membrane was washed for 5 min 3 times with TBS-T buffer, followed by incubation further with anti-mouse IgG, HRP-linked antibody (1:5,000) for iNOS and COX-2 or anti-rabbit IgG, HRP-linked antibody (1:5,000) for GAPDH diluted in blocking solution at room temperature with shaking

for 1 h. Next, the membrane was rinsed for 5 min 3 times with TBS-T buffer. The protein band on the PVDF membranes were detected on X-ray film using SuperSignal West Pico chemiluminescent. The X-ray film was washed with developer, water and fixer, respectively. The Image Studio Lite 5.2 Quick Start Guide program for Windows was used to determine the density of the band on X-ray film. The image densities of iNOS and COX-2 protein bands were normalized to the density of the GAPDH band.

3.2.6 Determination of mRNA expression by Quantitative reverse transcription-polymerase chain reaction (qRT-PCR)

3.2.6.1 Total RNA isolation using Nucleospin® RNA

BV2 microglial cells (1×10^6 cells/plate) were cultured in 60-mm plates at 37 ˚C in humidified air containing 5% CO_2 for 18-20 h. Then cells were pre-treated with fresh DMEM containing EPE at the concentrations of 25-100 µg/mL or MCC at the concentrations of 6.25-25 µM for 1 h before stimulating with LPS (1µg/mL) for 9 h for determination of iNOS and COX-2 mRNA, or 6 h for determination of TNF-α mRNA. Total RNA was extracted using NucleoSpin® RNA as directed by the manufacturer's instructions. Briefly, the cells were lysed in lysis buffer (350 µL of RA1 and 3.5 µL of β-mercaptoethanol). Then lysed cells were filtrated through a NucleoSpin® filter by centrifuged at 11,000 g for 1 min. The NucleoSpin® filter was removed, followed by adding 350 µL of 70% ethanol to the lysate. The lysate was pipetted up-and-down for 5 times, before pipetting into the NucleoSpin® RNA Column (light blue ring) that was placed in a new collection tube, followed by centrifugation for 30 sec at 11,000 g. Next, 350 µL of MDB (Membrane Desalting Buffer) was pipetted into the column before centrifugation at 11,000 g for 1 min. Afterward, 95 µL of DNase reaction mixture was pipetted directly onto the silica membrane center of each column and incubated for 15 min at room temperature. 200 µL of RA2 buffer was pipetted into the NucleoSpin® RNA Column before centrifugation for 30 sec at 11,000 g. The column was rinsed twice with 600 µL and 250 µL of RA3 buffer, respectively, followed by centrifuged at 11,000 g for 2 min. At the last step, RNA was eluted by 60 µL of RNase-free H_2O and centrifuged for 1 min at 11,000 g.

Total RNA concentration was assessed by measuring with a NanoDrop™ One Microvolume UV-Vis Spectrophotometer. The ratio of A_{260}/A_{280} was used in the range of 1.8-2.1, which indicates that the purity of RNA is wish.

3.2.6.2 Determination of mRNA expression by qRT-PCR

The total RNA was converted to cDNA by using a mixture containing 4 µL of 5x iScript™ Reverse Transcription (RT) Supermix for RT-qPCR [5x RT Supermix with RNase H^+ MML V-RT, RNase inhibitor, dNTPs, oligo (dT), random primers, buffer $MgCl_2$ and stabilizer], RNA template and nuclease-free water to make up volume 20 µL. The cDNA was synthesized under the conditions shown in table 3-2, using a CFX96 Touch™ Real-time PCR (Bio-Rad, USA).

Table 3-2 The conditions for cDNA synthesis

Reaction procedure	Temperature (˚C)	Time (min)
Priming	25	5
Reverse transcription	42	30
RT inactivation	85	5

The cDNA concentrations were determined by using NanoDrop™ One Microvolume UV-Vis Spectrophotometer.

Real time PCR was conducted on CFX96 Touch™ Real-time PCR. The PCR reaction contains 2x iTaq™ SYBR® Green Supermix [antibody-mediated hot-start iTaq™ DNA polymerase, dNTPs, $MgCl_2$, SYBR® Green I dye, enhancers, stablizers, blend of passive reference dyes], forward and reverse primer (10 µM), DNase-free water and cDNA (20 µL of final volume). The PCR condition is shown in table 3-3. The sequences of the PCR primers which were used for the iNOS, COX-2, TNF-α and elongation factor-2 (EF-2) are shown in table 3-4.

Table 3-3 The PCR cycling parameters

Gene	Cycle of amplification	Temperature (˚C)	Time (min)
iNOS, COX-2, TNF-α and EF-2	Stage 1: (1x) Step 1: for initial denaturation	95.0	3.00
	Stage 2: (40x) Step 1: for denaturation	95.0	0.10
	Stage 2: (40x) Step 2: for annealing	63.0	0.20
	Stage 4: (1x) Step 1: for extension	95.0	0.10

Table 3-4 The sequence of primer used in Real time RT-PCR (Mankhong, 2018)

Gene	Base sequences	Product size (bp)	Accession No.
iNOS	5’GCACAGCACAGGAAATGTTTCAGCAC3’ (F)	156	NM_010927.3
	5’AGCCAGCATACCGGATGAGC3’ (R)		
COX-2	5’TGATCGAAGACTACGTGCAACACC3’ (F)	164	NM_011198.3
	5’TTCAATGTTGAAGGTGTCGGGCAG3’ (R)		
TNF-α	5’CCCTCACACTCACAAACCACCA3’ (F)	186	NM_001278601.1
	5’TGAGGAGCACGTAGTCGGGG3’ (R)		
EF-2	5’CTGAAGCGGCTGGCTAAGTCTGA3’ (F)	155	NM_007907.3
	5’GGGTCAGATTTCTTGATGGGGATG3’ (R)		

Gene expression was analyzed by using the CFX manager™ software program. The value of the comparative cycle of threshold (Ct) was used to calculate relative gene expression using EF-2 as the housekeeping gene for normalization (Giulietti et al., 2001) as shown below.

$$2^{-\Delta\Delta C_T} = \text{Quantity of target gene}$$

$$\Delta C_T = [\text{average } C_T \text{ of target gene}] - [\text{average } C_T \text{ of housekeeping gene}]$$

$$\Delta\Delta C_T = [\text{average } \Delta C_T \text{ of treated cells}] - [\text{average } \Delta C_T \text{ of untreated cells}]$$

3.2.7 Determination of NF-κB activation

3.2.7.1 Whole cell extraction

BV2 microglial cells (1×10^6 cell/plate) were cultured in 60-mm plate for 18-20 h. Pre-treated cells with EPE at the concentrations of 25-100 µg/mL or MCC at the concentrations of 6.25-25 µM or 15 µM of BAY-117082 (a positive control) for 1 h before being LPS (1µg/mL) stimulated. After 30 min, the cultured media was discarded and rinsed with cold PBS for twice. Then cells were scraped on ice with 150 µL of cold RIPA protein lysis buffer containing 1x phosphatase inhibitor cocktail, 1x protease inhibitor cocktail and 1mM DTT. The cell lysate was centrifuged at 13,700 g for 10 min at 4 ˚C and supernatant was collected to a new microcentrifuge tube. After that, protein concentration in the supernatant was estimated by the Bradford protein assay as described in section 3.3.5.2.

3.2.7.2 Western blot analysis

The protein was separated onto 10% SDS-PAGE in equal amounts and electrotransferred to the PVDF membrane as described in section 3.3.5.3. Then, the membrane was blocked by incubation for 1 h with blocking solution before incubating with primary antibodies under the conditions shown in table 3-5.

Table 3-5 The conditions of incubation for phospho-IκBα, phospho-NF-κB p65 and GAPDH primary antibodies

Protein	Fold of dilution	Dissolvent	Time	Temperature
phospho-IκBα	1:1,000	5% (w/v) skim milk, 1x TBS, 0.1% Tween® 20	Overnight	4 ˚C
phospho-NF-κB p65	1:1,000	5% (w/v) BSA, 1x TBS, 0.1% Tween® 20		
GAPDH	1:1,000	5% (w/v) BSA, 1x TBS, 0.1% Tween® 20	1 h	Room temp.

Afterward, the membrane was rinsed with TBS-T buffer for 5 min 3 times, and incubated with anti-mouse IgG, HRP-linked antibody (1:5,000) for phospho-IκBα or anti-rabbit IgG, HRP-linked antibody (1:5,000) for phospho-NF-κB p65 or GAPDH, which were dissolved in blocking solution at room temperature with shaking for 1 h. Later, the membrane was rinsed with TBS-T buffer for 5 min 3 times. The protein band on the PVDF membrane was detected on X-ray film using SuperSignal West Pico chemiluminescent. The X-ray film was washed with developer, water and fixer, respectively. The protein bands on X-ray film were determined density using the Image Studio Lite 5.2 Quick Start Guide program for windows. The image densities of protein bands for phospho-NF-κB p65 and phospho-IκBα were normalized with a density of the GAPDH band.

3.2.8 Determination of MAPKs phosphorylation

3.2.8.1 Whole cell extraction

BV2 microglial cells were plated into 60-mm plate (1×10^6 cells/plate) and incubated at 37 ˚C for 18-20 h. The cells were pre-treated with DMEM containing MCC at the concentrations of 6.25-25 μM for 1 h before being LPS (1μg/mL) stimulated for 30 min. Then, the cells were rinsed twice with cold PBS (1x), before being scraped on ice with 150 μL of cold RIPA protein lysis buffer mixed with 1x phosphatase inhibitor cocktail, 1x protease inhibitor cocktail and 1 mM DTT. The cell lysates were centrifuged at 13,700 g for 10 min at 4 ˚C, and the supernatant was

collected into a new microcentrifuge tube. After that, protein concentrations in the supernatant were assessed by the Bradford protein assay as stated in section 3.3.5.2.

3.2.8.2 Western blot analysis

Equal amount of proteins was evaluated by western blot analysis as stated in section 3.3.5.3. Then, the membrane was incubated with blocking solution for 1 h with shaking at room temperature before being incubated further with primary antibodies as shown in the table 3-6.

Table 3-6 The conditions of incubation for phospho-ERK1/2, phospho-JNK, phospho-p38, ERK1/2, JNK and p38 primary antibodies

<table>
<tr><th>Protein</th><th>Fold of dilution</th><th>Dissolvent</th><th>Time</th><th>Temperature</th></tr>
<tr><td>phospho-ERK1/2</td><td>1:1,000</td><td rowspan="4">5% (w/v) BSA, 1x TBS, 0.1% Tween® 20</td><td rowspan="6">Overnight</td><td rowspan="6">4 ˚C</td></tr>
<tr><td>phospho-JNK</td><td>1:1,000</td></tr>
<tr><td>phospho-p38</td><td>1:1,000</td></tr>
<tr><td>JNK</td><td>1:1,000</td></tr>
<tr><td>ERK1/2</td><td>1:2,000</td><td rowspan="2">0.5% (w/v) BSA in PBS, 0.05% (v/v) Tween® 20</td></tr>
<tr><td>p38</td><td>1:1,000</td></tr>
</table>

The membrane was rinsed 5 min 3 times with TBS-T buffer before incubating with anti-rabbit IgG, HRP-linked antibody (1:5,000) for phospho-ERK1/2, phospho-JNK, ERK1/2, JNK and p38 and anti-rabbit IgG, HRP-linked antibody (1:2,000) for phospho-p38 dissolved in blocking solution at room temperature for 1 h. The membrane was rinsed with TBS-T buffer for 5 min 3 times. The protein band on the PVDF membrane was detected on X-ray film using SuperSignal West Pico chemiluminescent. The X-ray film was washed with developer, water and fixer,

respectively. The protein bands on X-ray film were determined density using the Image Studio Lite 5.2 Quick Start Guide program for windows. The image densities of protein bands for phospho-ERK1/2, phospho-JNK and phospho-p38 were normalized using a density of their total protein bands.

3.2.9 Statistical analysis

The data were presented as the means±S.D. of at least three times independent experiments. Minitab 18 for Windows was used to analyze the data for statistical significance. The statistical significance of the difference in extract concentration was assessed via one-way analysis of variance (ANOVA), followed by Tukey's test for multiple comparison. A value of $p<0.05$ was considered to be significant.

CHAPTER 4
RESULTS

4.1 Anti-neuroinflammatory effects of EPE on BV2 microglial cells

4.1.1 Effect of EPE on cell viability of BV2 microglial cells

The cytotoxicity of EPE was determined by MTT assay. BV2 microglial cells were treated with EPE alone at the concentrations of 6.25-200 µg/mL for 24 h. EPE at concentration 200 µg/mL significantly decreased cell viability from unstimulated control cells (Figure 4-1A). EPE at the concentrations of 6.25-100 µg/mL did not significantly altered the cell viability. Furthermore, EPE at the concentrations of 6.25-100 µg/mL did not significantly change %viability of LPS-treated cells compared with unstimulated control cells (Figure 4-1B). Thus, EPE at concentrations up to 100 µg/mL were used for the further experiments.

4.1.2 Effect of EPE on NO production in LPS-stimulated BV2 microglial cells

NO produced by activated microglial cells was released outside the cells and rapidly oxidized to nitrite and accumulated in the culture media. As a result, nitrite was used as an index for measuring the amount of NO production. Nitrite concentration in culture media of unstimulated cells was -0.08±0.18 µM (Figure 4-2A). After 24 h, the concentration of nitrite in LPS-stimulated cells was 12.67±0.54 µM, substantially increased when compared with unstimulated control cells. Meanwhile, NO production in EPE-pretreated cells was considerably reduced in a concentration-dependent manner. The inhibitory effect of EPE on NO production in LPS-stimulated cells had an IC_{50} value of 52.10±1.78 µg/mL. Aminoguanidine, a particular inhibitor of iNOS activity, was utilized as a positive control. AG at a concentration of 50 µM significantly inhibited LPS-stimulated NO production by 78.59±4.33% (Figure 4-2B).

(A)

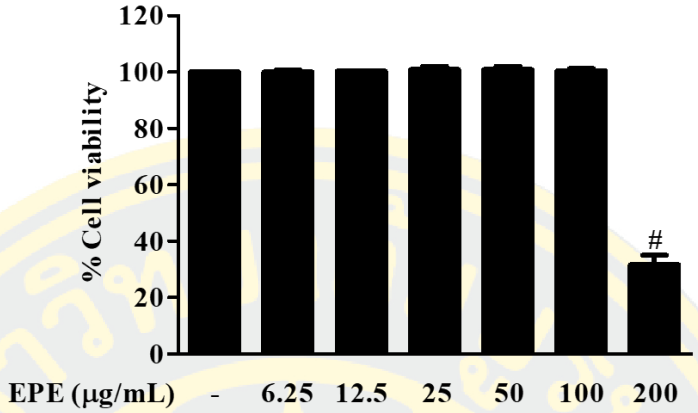

(B)

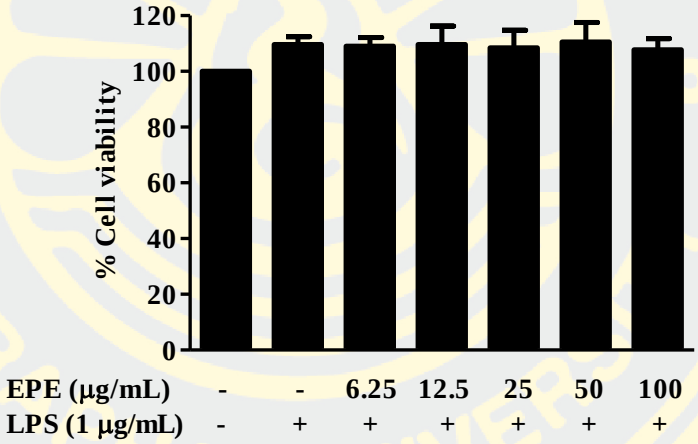

Figure 4-1 The effect of EPE on cell viability of BV2 microglial cells. Cells were treated with EPE at the concentrations of 6.25-200 µg/mL for 24 h (A) and treated with EPE at the concentrations of 6.25-100 µg/mL in the presence of LPS (1 µg/mL) for 24 h (B). Each column shows a mean±SD of at least three independent experiments with triplicated samples. #$p<0.05$ compared with unstimulated control cells.

(A)

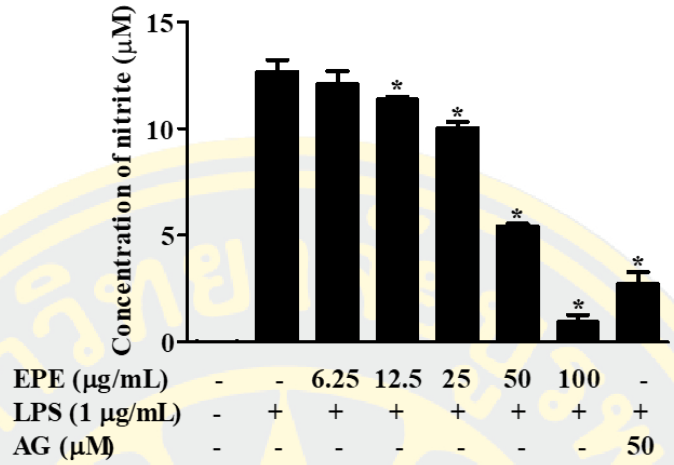

(B)

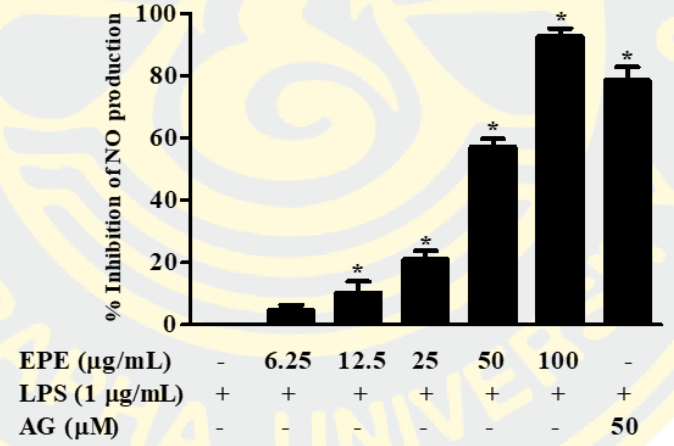

Figure 4-2 Concentration of nitrite (A) and percent inhibition of NO production (B) in culture media of LPS-stimulated BV2 microglial cells. Cells were pre-treated with EPE at the concentrations of 6.25-100 µg/mL and 50 µM of aminoguanidine (AG) for 1 h before stimulating with 1 µg/mL of LPS for 24 h. Each column shows a mean±SD of at least three independent experiments with triplicated samples. #$p<0.05$ compared with unstimulated control cells and *$p<0.05$ compared with LPS-stimulated cells.

4.1.3 Effect of EPE on iNOS expression in LPS-stimulated BV2 microglial cells

iNOS is well known to catalyze the synthesis of NO from L-arginine in activated microglial cells. To investigate whether the inhibitory activity of EPE on NO production was related to the expression of iNOS, Western blot and qRT-PCR were used to quantify the amount of protein and mRNA, respectively. As shown in Figure 4-3 and Figure 4-4, the protein and mRNA levels of iNOS were hardly detectable in unstimulated control cells. The stimulation of cells with 1 μg/mL LPS resulted in a considerable increased in iNOS protein levels compared with unstimulated control cells. On the other hand, pretreatment of cells with EPE significantly suppressed the expression level of iNOS protein in a concentration-dependent manner (Figure 4-3). The GAPDH protein, used as an internal control, was not significantly affected by LPS and EPE treatment. In addition, the level of iNOS mRNA was significantly increased above the control level after stimulating with 1 μg/mL of LPS for 9 h. EPE markedly suppressed the iNOS mRNA expression level in a concentration-dependent manner (Figure 4-4). To normalize the level of iNOS mRNA, the level of EF-2 mRNA was employed as an internal control. The reduced iNOS protein expression was associated with the suppression of iNOS mRNA level and also related with the production of NO.

4.1.4 Effect of EPE on PGE_2 production in LPS-stimulated BV2 microglial cells

To determine the effect of EPE on PGE_2 production in LPS-stimulated BV2 microglial cells. Cells were pre-treated for 1 h with various concentrations of EPE before being stimulated with 1 μg/mL of LPS. The amount of PGE_2 in the culture media was determined using a competitive enzyme immunoassay kit. PGE_2 concentration in culture media of unstimulated cells was 7370.67±578.56 pg/mL (Figure 4-5A). PGE_2 production were significantly higher in LPS-treated cells than in unstimulated control cells, up to 10952.32±637.90 pg/mL. EPE significantly inhibited PGE_2 production in a concentration-dependent manner. The IC_{50} value of EPE on PGE_2 production in LPS-stimulated cells was 37.32±6.92 μg/mL. Indomethacin (IMC), a COX-2 inhibitor employed as a positive control and suppressed PGE_2 production by 95.13±1.67% at the concentration of 1 μM (Figure 4-5B).

(A)

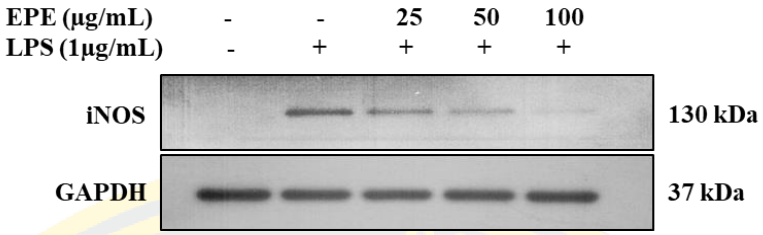

(B)

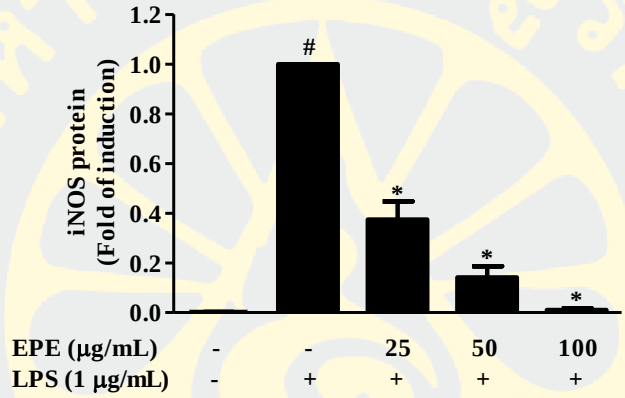

Figure 4-3 Effect of EPE on iNOS protein expression in LPS- stimulated BV2 microglial cells. Cells were pre-treated with EPE at the concentrations of 25-100 µg/mL for 1 h before stimulating with 1 µg/mL of LPS for 24 h. The level of iNOS protein expression was determined by Western blot analysis (A). Each column shows a mean±SD of densitometric values determined by Image Studio Lite 5.2 Quick Start Guide program and normalized with GAPDH (B). Data are expressed as a fold change with respect to cells treated with LPS only. #$p<0.05$ compared with unstimulated control cells and *$p<0.05$ compared with LPS-stimulated cells.

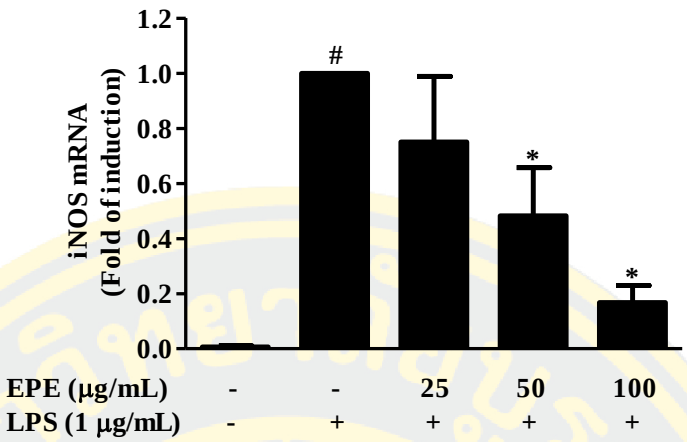

Figure 4-4 Effect of EPE on iNOS mRNA expression in LPS-stimulated BV2 microglial cells. Cells were pre-treated with EPE at the concentrations of 25-100 µg/mL for 1 h before stimulating with 1 µg/mL of LPS for 9 h. The expression of iNOS mRNA was determined by qRT-PCR and normalized with EF-2. Each column shows a mean±SD of three independent experiments. Data are expressed as a fold change with respect to cells treated with LPS only. #$p<0.05$ compared with unstimulated control cells and *$p<0.05$ compared with LPS-stimulated cells.

(A)

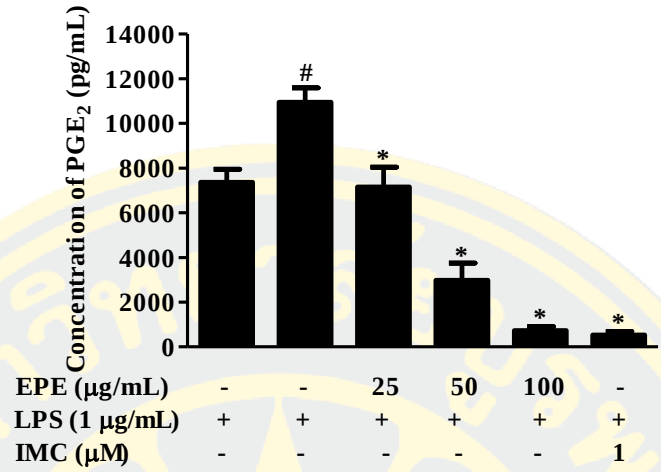

(B)

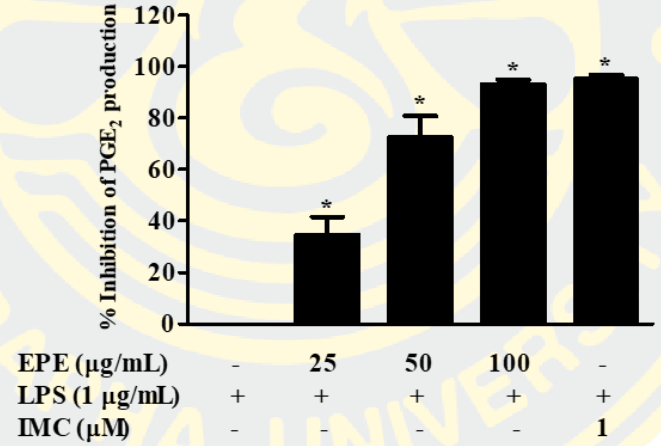

Figure 4-5 Concentration of PGE_2 (A) and percent inhibition of PGE_2 production (B) in culture media of LPS-stimulated BV2 microglial cells. Cells were pre-treated with EPE at the concentrations of 25-100 µg/mL and 1 µM of indomethacin (IMC) for 1 h before stimulating with 1 µg/mL of LPS for 24 h. Each column shows a mean±SD of at least three independent experiments with duplicated samples. #p<0.05 compared with unstimulated control cells and *p<0.05 compared with LPS-stimulated cells.

4.1.5 Effect of EPE on COX-2 expression in LPS-stimulated BV2 microglial cells

As shown in Figure 4-5, EPE inhibited the production of PGE_2. Thus, to describe the inhibitory activity of EPE on PGE_2 production, the expression of protein and mRNA were quantified by Western blot and qRT-PCR, respectively. The protein levels of COX-2 were considerably increased in cells stimulated with 1 µg/mL of LPS (Figure 4-6). Nevertheless, pretreatment of cells with EPE at the concentrations of 50-100 µg/mL significantly suppressed the expression level of COX-2 protein in a concentration-dependent manner. The GAPDH protein was unaffected by LPS and EPE treatment used as an internal control. Moreover, the mRNA level of COX-2 was markedly increased above the control level after stimulating with 1 µg/mL of LPS (Figure 4-7). However, the level of COX-2 mRNA was significantly suppressed by pretreatment cells with EPE at concentration 100 µg/mL. The level of EF-2 mRNA was used as an internal control to normalize the level of COX-2 mRNA. The effect of EPE on COX-2 protein and mRNA expression were related and also coordinated with PGE_2 production.

4.1.6 Effect of EPE on NF-κB activation in LPS-stimulated BV2 microglial cells

Since EPE exhibited the inhibitory effect on LPS-stimulated iNOS and COX-2 expression, we determined whether such inhibitory effect might be occurring through activation of NF-κB signaling pathway. The effect of EPE were investigated on signal cascades beginning with LPS-stimulated phosphorylation of IκBα protein by Western blot analysis. The level of phosphorylated IκBα protein was markedly increased after stimulating with 1 µg/mL of LPS for 30 min (Figure 4-8). While, EPE-pretreatment cells significantly suppressed LPS-stimulated phosphorylation of IκBα. In addition, the phosphorylation of NF-κB p65 was determined by Western blot analysis. Western blot data as shown in Figure 4-9 markedly revealed that LPS caused a prominent induction of phosphorylation of NF-κB p65 protein. However, pretreatment of cells with EPE at the concentrations of 50-100 µg/mL significantly reduced LPS-stimulated phosphorylation of NF-κB p65. A NF-κB activation inhibitor, BAY 11-7082, was used as a positive control.

(A)

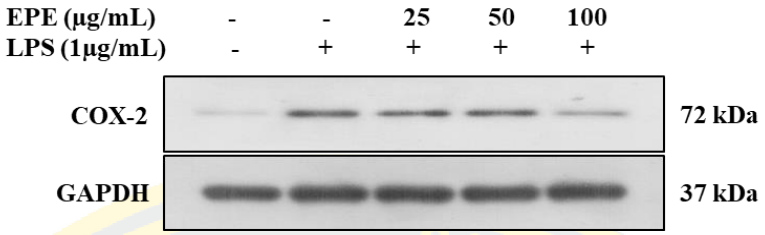

(B)

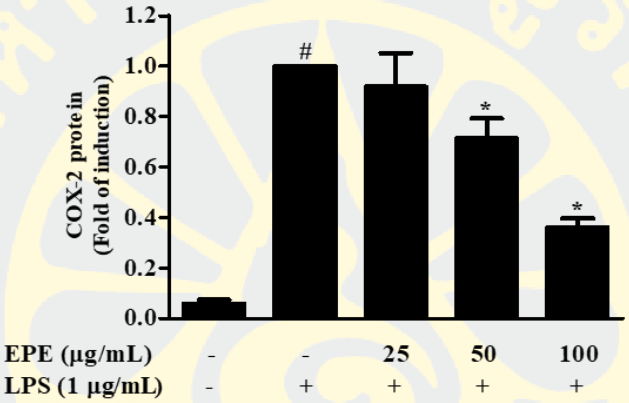

Figure 4-6 Effect of EPE on COX-2 protein expression in LPS-stimulated BV2 microglial cells. Cells were pre-treated with EPE at the concentrations of 25-100 µg/mL for 1 h before stimulating with 1 µg/mL of LPS for 24 h. The level of COX-2 protein expression was determined by Western blot analysis (A). Each column shows a mean±SD of densitometric values determined by Image Studio Lite 5.2 Quick Start Guide program and normalized with GAPDH (B). Data are expressed as a fold change with respect to cells treated with LPS. #$p<0.05$ compared with unstimulated control cells and *$p<0.05$ compared with LPS-stimulated cells.

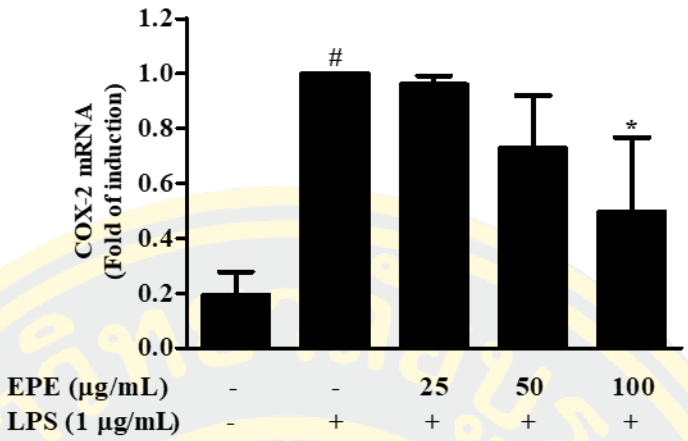

Figure 4-7 Effect of EPE on COX-2 mRNA expression in LPS-stimulated BV2 microglial cells. Cells were pre-treated with EPE at the concentrations of 25-100 µg/mL for 1 h before stimulating with 1 µg/mL of LPS for 9 h. The expression of COX-2 mRNA was investigated by qRT-PCR and normalized with EF-2. Each column shows a mean±SD of three independent experiments. Data are expressed as a fold change with respect to cells treated with LPS. #$p<0.05$ compared with unstimulated control cells and *$p<0.05$ compared with LPS-stimulated cells.

(A)

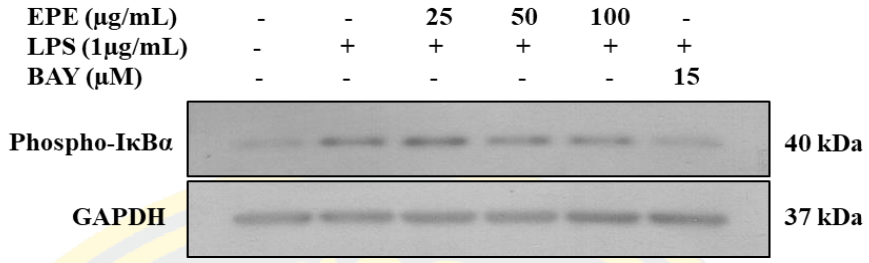

(B)

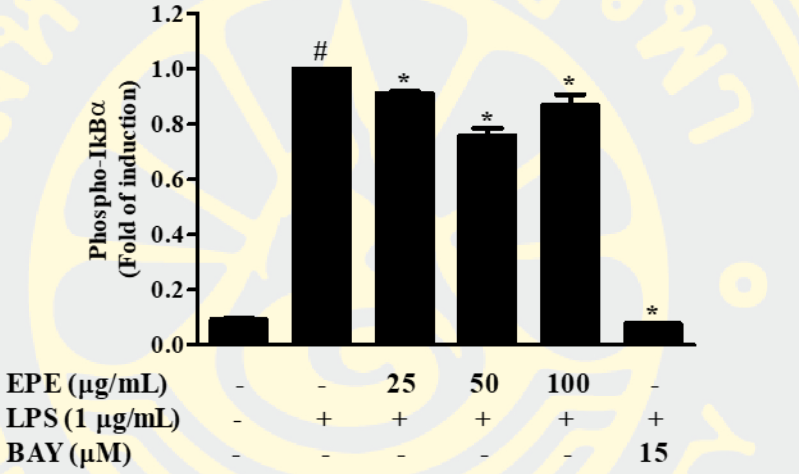

Figure 4-8 Effect of EPE on IκBα phosphorylation in LPS-stimulated BV2 microglial cells. Cells were pre-treated with EPE at the concentrations of 25-100 µg/mL and 15 µM of BAY 11-7082 (BAY) for 1 h before stimulating with 1 µg/mL of LPS for 30 min. Total protein was determined by Western blot analysis (A). Each column shows a mean±SD of densitometric values determined by Image Studio Lite 5.2 Quick Start Guide program and the phospho-IκBα were normalized with GAPDH (n=3) (B). Data are expressed as a fold change of LPS-stimulated cells. #p<0.05 compared with unstimulated control cells and *p<0.05 compared with LPS-stimulated cells.

(A)

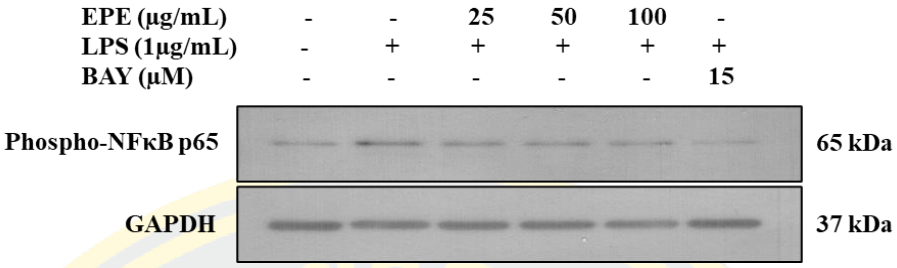

(B)

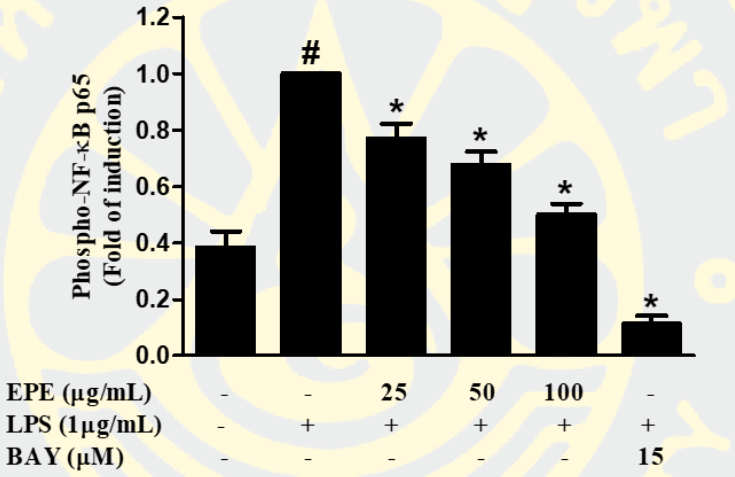

Figure 4-9 Effect of EPE on NF-κB p65 phosphorylation in LPS-stimulated BV2 microglial cells. Cells were pre-treated with EPE at the concentrations of 25-100 µg/mL and 15 µM of BAY 11-7082 (BAY) for 1 h before stimulating with 1 µg/mL of LPS for 30 min. Total protein was determined by Western blot analysis (A). Each column shows a mean±SD of densitometric values determined by Image Studio Lite 5.2 Quick Start Guide program and the phospho-NF-κB p65 were normalized with GAPDH (n=3) (B). Data are expressed as a fold change of LPS-stimulated cells. #p<0.05 compared with unstimulated control cells and *p<0.05 compared with LPS-stimulated cells.

4.2 Anti-neuroinflammatory effects of MCC on BV2 microglial cells

4.2.1 Effect of MCC on cell viability of BV2 microglial cells

BV2 microglial cells were treated with MCC alone at the concentrations of 6.25-200 µM for 24 h. MCC at the concentrations of 50-200 µM significantly decreased the cell viability compared with unstimulated control cells (Figure 4-10A). Conversely, MCC at concentration 6.25-25 µM did not significantly change the cell viability. Additionally, MCC at concentration 6.25-25 µM did not significantly altered cell viability in the presence of 1 µg/mL LPS compared with unstimulated control cells (Figure 4-10B). Thus, MCC at the concentration up to 25 µM were used in further experiments.

4.2.2 Effect of MCC on NO production in LPS-stimulated BV2 microglial cells

To examine the inhibitory effect of MCC on NO production, BV2 microglial cells were treated with MCC at the concentrations of 6.25-25 µM and LPS. Nitrite concentration in culture media of unstimulated cells was 0.29±0.08 µM (Figure 4-11A). While the concentration of nitrite was enhanced up to 9.43±1.72 µM when stimulation with 1 µg/mL LPS for 24 h compared with unstimulated control cells. Pretreatment with MCC, the production of NO was substantially reduced in a concentration-dependent manner. The IC_{50} value of MCC on NO production in LPS-stimulated cells was 3.32±1.13 µM. A positive control AG at the concentration of 50 µM could inhibit LPS-stimulated NO production by 74.76±3.10% (Figure 4-11B).

(A)

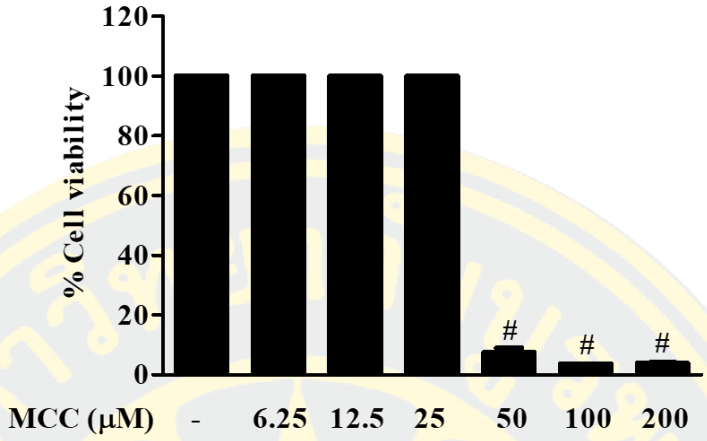

(B)

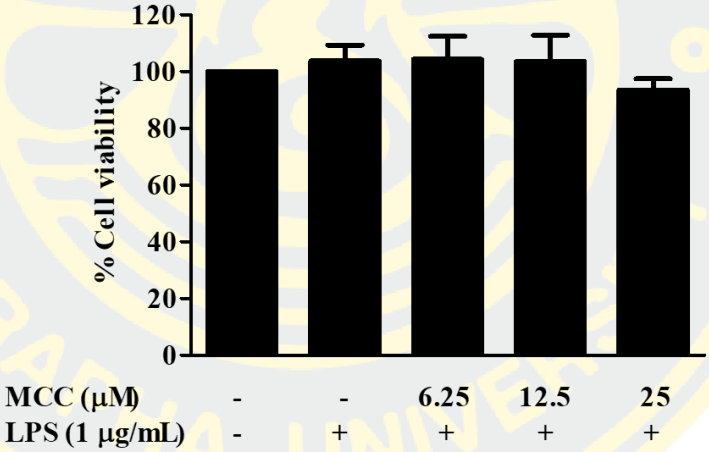

Figure 4-10 The effect of MCC on cell viability of BV2 microglial cells. Cells were treated with MCC at the concentrations of 6.25-200 μM for 24 h (A) and treated with MCC at the concentrations of 6.25-25 μM in the presence of LPS (1 μg/mL) for 24 h. (B). Each column shows a mean±SD of at least three independent experiments with triplicated samples. #$p<0.05$ compared with unstimulated control cells.

(A)

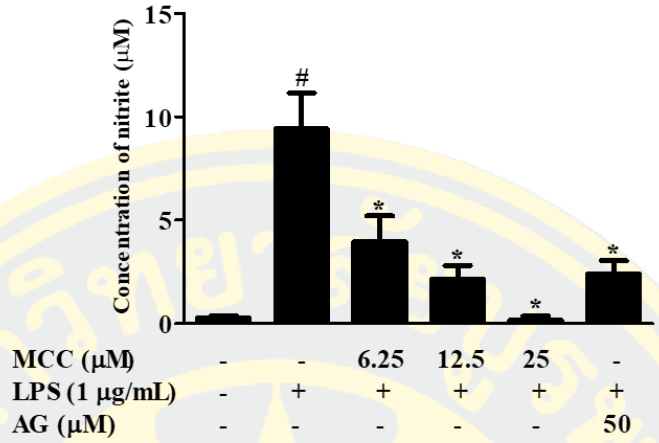

(B)

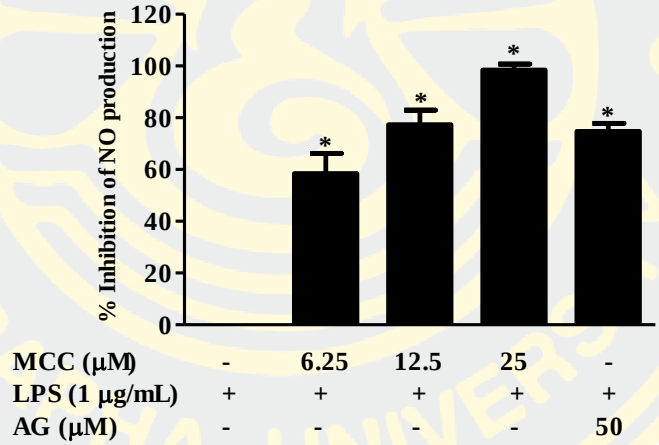

Figure 4-11 Concentration of nitrite (A) and percent inhibition of NO production (B) in culture media of LPS-stimulated BV2 microglial cells. Cells were pre-treated with MCC at the concentrations of 6.25-25 μM and 50 μM of aminoguanidine (AG) for 1 h before stimulating with 1 μg/mL LPS for 24 h. Each column shows a mean±SD of at least three independent experiments with triplicated samples. #$p<0.05$ compared with unstimulated control cells and *$p<0.05$ compared with LPS-stimulated cells.

4.2.3 Effect of MCC on iNOS expression in LPS-stimulated BV2 microglial cells

The levels of iNOS protein and mRNA were quantified by using Western blot and qRT-PCR, respectively. The expression of iNOS protein was highly induced in cells stimulated with 1 µg/mL LPS for 24 h compared with unstimulated control cells. However, MCC significantly decreased the level of iNOS protein expression in a concentration-dependent manner (Figure 4-12). The GAPDH protein synthesis was unaffected by LPS and MCC treatment. Besides, the level of iNOS mRNA was significantly increased after stimulating with LPS compared with unstimulated control cells. Anywise, pre-treatment cells with MCC markedly reduced the expression level of iNOS mRNA in a concentration-dependent manner (Figure 4-13).

4.2.4 Effect of MCC on PGE_2 production in LPS-stimulated BV2 microglial cells

The amount of PGE_2 in the culture media was examined by using a competitive enzyme immunoassay kit. PGE_2 concentration in culture media of unstimulated cells was 7905.51±1412.32 pg/mL (Figure 4-14A). PGE_2 production were significantly increased up to 10375.92±1809.51 pg/mL when cells stimulated with 1 µg/mL of LPS. MCC-pretreatment cells significantly decreased PGE_2 production in a concentration-dependent manner with IC_{50} value of 13.32±2.18 µM. A positive control IMC at a concentration of 1 µM could suppress LPS-stimulated PGE_2 production by 93.47.76±2.34% (Figure 4-14B).

(A)

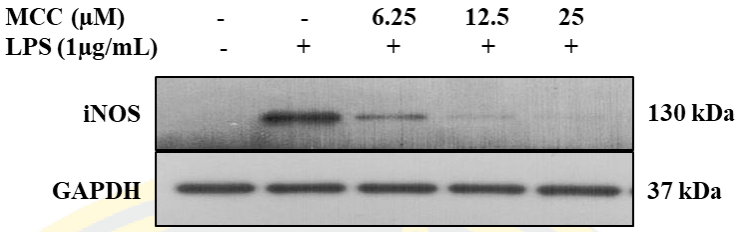

(B)

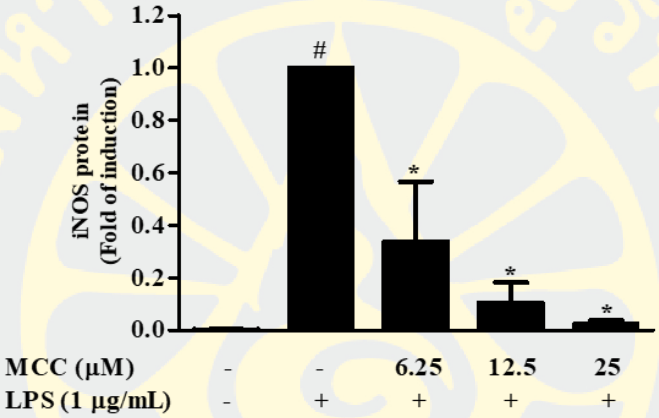

Figure 4-12 Effect of MCC on iNOS protein expression in LPS- stimulated BV2 microglial cells. Cells were pre-treated with MCC at the concentrations of 6.25-25 μM for 1 h before stimulating with 1 μg/mL LPS for 24 h. The level of iNOS protein expression was determined by Western blot analysis (A). Each column shows a mean±SD of densitometric values determined by Image Studio Lite 5.2 Quick Start Guide program and normalized with GAPDH (B). Data are expressed as a fold change with respect to cells treated with LPS only. #$p<0.05$ compared with unstimulated control cells and *$p<0.05$ compared with LPS-stimulated cells.

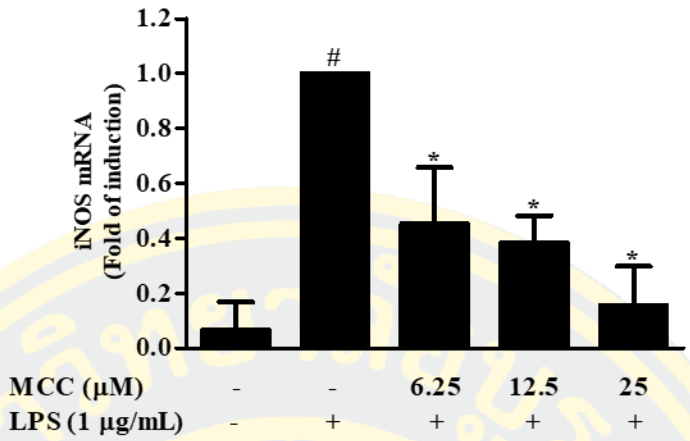

Figure 4-13 Effect of MCC on iNOS mRNA expression in LPS-stimulated BV2 microglial cells. Cells were pre-treated with MCC at the concentrations of 6.25-25 µM for 1 h before stimulating with 1 µg/mL LPS for 9 h. The expression of iNOS mRNA was determined by qRT-PCR and normalized with EF-2. Each column shows a mean±SD of three independent experiments. Data are expressed as a fold change with respect to cells treated with LPS only. #$p<0.05$ compared with unstimulated control cells and *$p<0.05$ compared with LPS-stimulated cells.

(A)

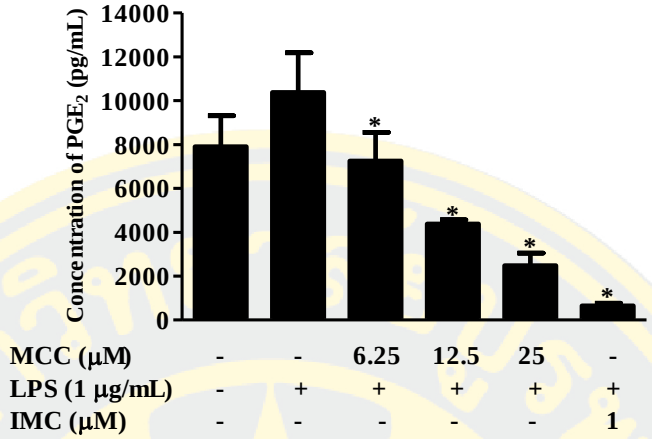

(B)

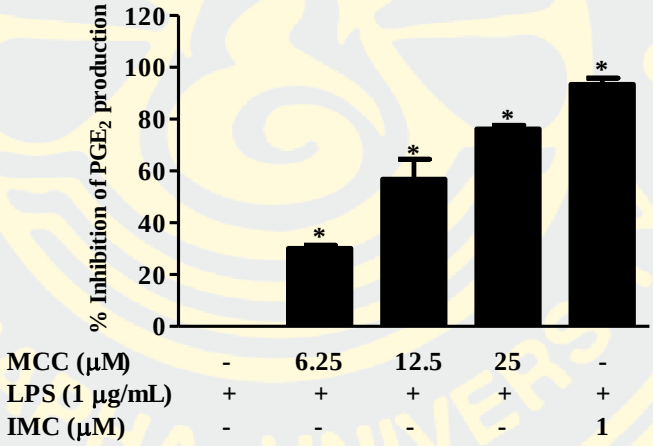

Figure 4-14 Concentration of PGE_2 (A) and percent inhibition of PGE_2 production (B) in culture media of LPS-stimulated BV2 microglial cells. Cells were pre-treated with MCC at the concentrations of 6.25-25 μM and 1 μM of indomethacin (IMC) for 1 h before stimulating with 1 μg/mL LPS for 24 h. Each column shows a mean±SD of at least three independent experiments with duplicated samples. #p<0.05 compared with unstimulated control cells and *p<0.05 compared with LPS-stimulated cells.

4.2.5 Effect of MCC on COX-2 expression in LPS-stimulated BV2 microglial cells

LPS stimulation caused higher induction of COX-2 protein level (Figure 4-15). The result showed that, pretreatment of cells with MCC at concentration 25 µM significantly reduced the expression level of COX-2 protein. Likewise, the mRNA level of COX-2 was significantly increased from the control level when exposed to LPS (Figure 4-16). MCC at the concentration of 25 µM significantly suppressed LPS-stimulated COX-2 mRNA expression.

4.2.6 Effect of MCC on TNF-α production in LPS-stimulated BV2 microglial cells

To investigated the effect of MCC on TNF-α production in LPS-stimulated BV2 microglial cells, cells were pre-treated for 1 h with MCC at the concentrations of 6.25-25 µM before stimulated with 1 µg/mL of LPS. After 24 h, culture medium was collected to measured TNF-α production by using mouse TNF-α quantikine ELISA kit. The concentration of TNF-α production in the culture media of unstimulated cells was 418.40±29.69 pg/mL and enhanced to 817.65±42.14 pg/mL in LPS-stimulated cells (Figure 4-17A). However, MCC at the concentrations of 12.5-25 µM were significantly decreased TNF-α production with an IC_{50} value of 36.01±14.47 µM.

4.2.7 Effect of MCC on TNF-α expression in LPS-stimulated BV2 microglial cells

The mRNA expression of TNF-α was evaluated by qRT-PCR. As shown in Figure 4-18, LPS stimulation induced the large of TNF-α mRNA expression compared with unstimulated cells. MCC at the concentrations of 12.5-25 µM significantly reduced LPS-stimulated TNF-α mRNA expression. The EF-2 mRNA level was used as an internal control to compare the level of TNF-α mRNA expression.

(A)

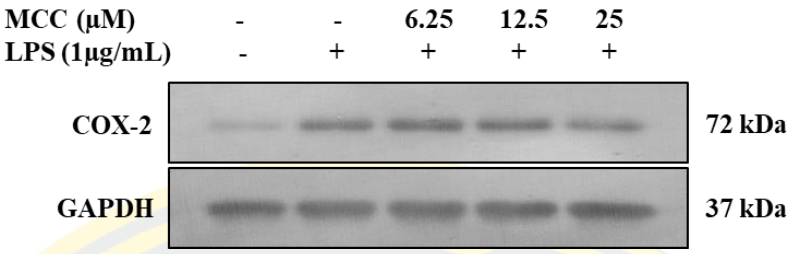

(B)

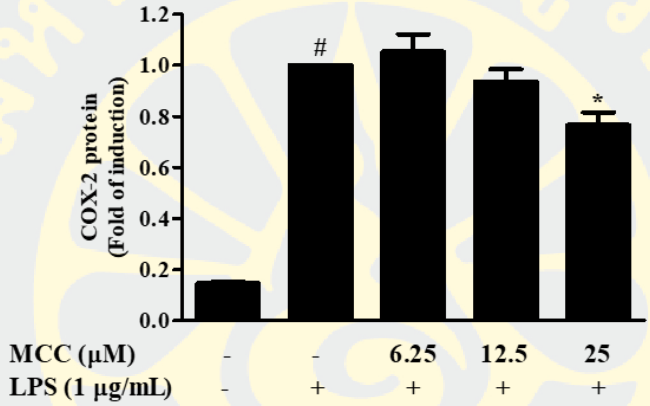

Figure 4-15 Effect of MCC on COX-2 protein expression in LPS-stimulated BV2 microglial cells. Cells were pre-treated with MCC at the concentrations of 6.25-25 μM for 1 h before stimulating with 1 μg/mL LPS for 24 h. The level of COX-2 protein expression was determined by Western blot analysis (A). Each column shows a mean±SD of densitometric values determined by Image Studio Lite 5.2 Quick Start Guide program and normalized with GAPDH (B). Data are expressed as a fold change with respect to cells treated with LPS. #$p<0.05$ compared with unstimulated control cells and *$p<0.05$ compared with LPS-stimulated cells.

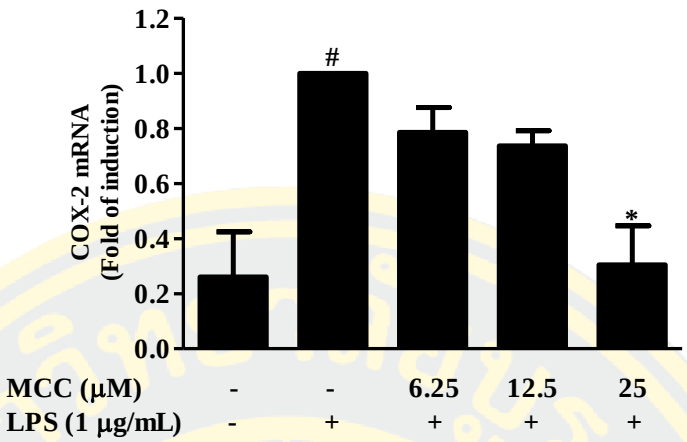

Figure 4-16 Effect of MCC on COX-2 mRNA expression in LPS-stimulated BV2 microglial cells. Cells were pre-treated with MCC at the concentrations of 6.25-25 µM for 1 h before stimulating with 1 µg/mL LPS for 9 h. The expression of COX-2 mRNA was examined by qRT-PCR and normalized with EF-2. Each column shows a mean±SD of three independent experiments. Data are expressed as a fold change with respect to cells treated with LPS. #$p<0.05$ compared with unstimulated control cells and *$p<0.05$ compared with LPS-stimulated cells.

(A)

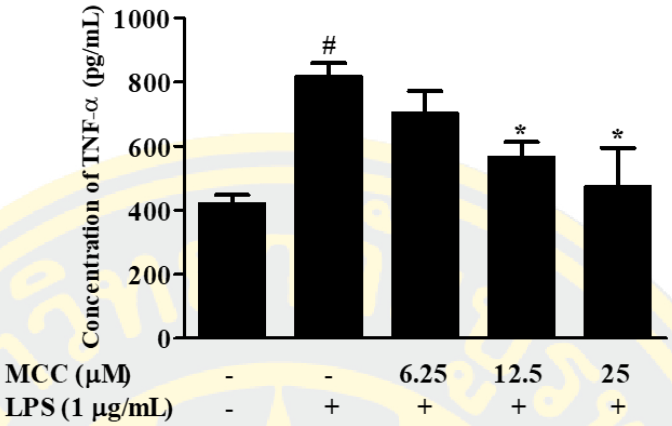

(B)

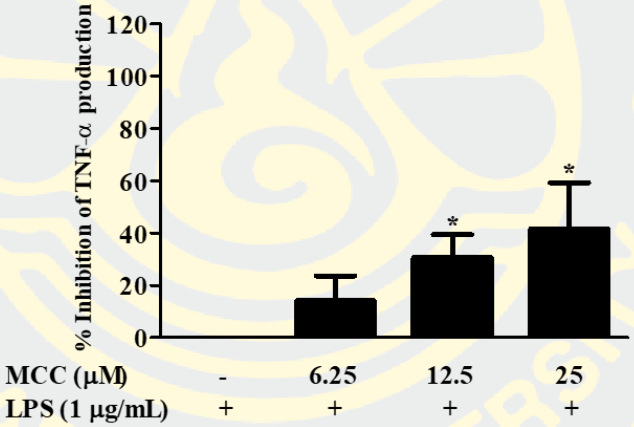

Figure 4-17 Concentration of TNF-α (A) and percent inhibition of TNF-α production (B) in LPS-stimulated BV2 microglial cells. Cells were pre-treated with MCC at the concentrations of 6.25-25 μM for 1 h before stimulating with 1 μg/mL LPS for 24 h. Each column shows a mean±SD of at least three independent experiments with duplicated samples. #$p<0.05$ compared with unstimulated control cells and *$p<0.05$ compared with LPS-stimulated cells.

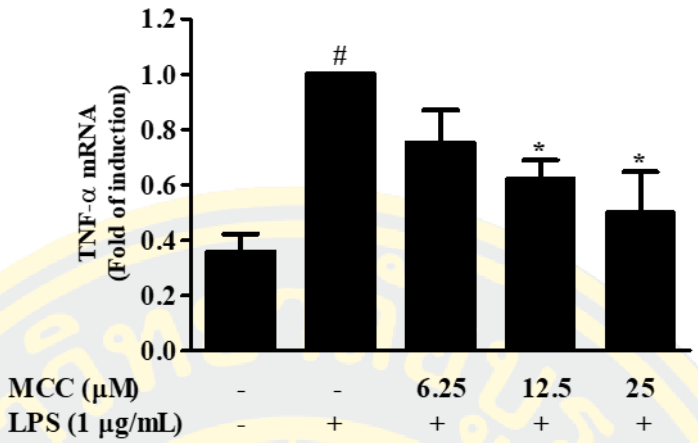

Figure 4-18 Effect of MCC on TNF-α mRNA expression in LPS-stimulated BV2 microglial cells. Cells were pre-treated with MCC at the concentrations of 6.25-25 μM for 1 h before stimulating with 1 μg/mL of LPS for 6 h. The expression of TNF-α mRNA was examined by qRT-PCR and normalized with EF-2. Each column shows a mean±SD of three independent experiments. Data are expressed as a fold change with respect to cells treated with LPS only. #$p<0.05$ compared with unstimulated control cells and *$p<0.05$ compared with LPS-stimulated cells.

4.2.8 Effect of MCC on NF-κB activation in LPS-stimulated BV2 microglial cells

As shown in Figure 4-19 and 4-20, LPS induced a markedly increased of phosphorylated IκBα and NF-κB p65 protein levels compared to unstimulated cells. MCC at the concentrations of 6.25-25 μM significantly suppressed LPS-stimulated phosphorylation of IκBα protein levels in a concentration-dependent manner (Figure 4-19). Moreover, MCC significantly reduced LPS-stimulated phosphorylation of NF-κB p65 (Figure 4-20). BAY 11-7082, a NF-κB activation inhibitor, used as a positive control.

4.2.9 Effect of MCC on phosphorylation of MAP kinases in LPS-stimulated BV2 microglial cells

To further explore the molecular mechanism underlying the inhibitory effect of MCC on LPS-induced microglial cells. Another signaling pathway, MAPKs were investigated by Western blot analysis. The phosphorylation level of p38, ERK1/2 and JNK significantly increased after being stimulated with LPS for 30 min compared with unstimulated cells (Figure 4-21, 4-22 and 4-23). MCC at the concentrations of 6.25-25 μM significantly reduced the phosphorylation of p38 (Figure 4-21), while MCC at the concentrations of 12.5-25 μM significantly reduced the phosphorylation of JNK (Figure 4-23). Furthermore, MCC obviously enhanced the phosphorylation of ERK1/2 (Figure 4-22).

(A)

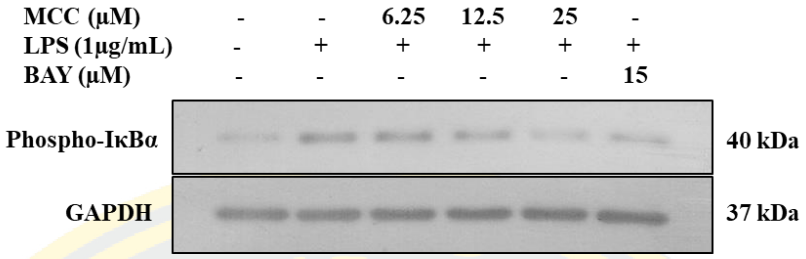

(B)

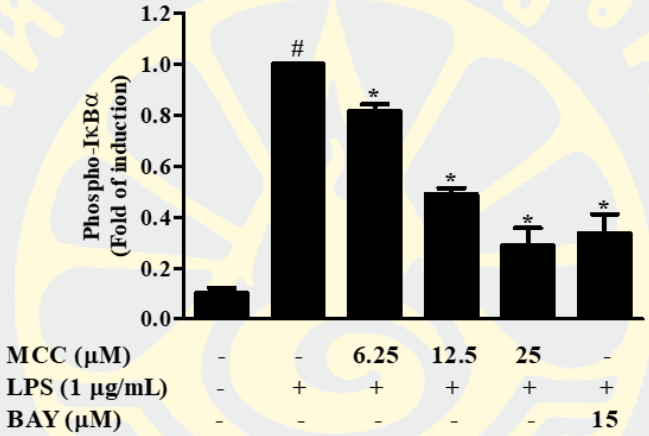

Figure 4-19 Effect of MCC on IκBα phosphorylation in LPS-stimulated BV2 microglial cells. Cells were pre-treated with MCC at the concentrations of 6.25-25 μM for 1 h before stimulating with 1 μg/mL LPS for 30 min. Total protein was determined by Western blot analysis (A). Each column shows a mean±SD of densitometric values determined by Image Studio Lite 5.2 Quick Start Guide program and the phospho-IκBα were normalized with GAPDH (n=3) (B). Data are expressed as a fold change of LPS-stimulated cells. #p<0.05 compared with unstimulated control cells and *p<0.05 compared with LPS-stimulated cells.

(A)

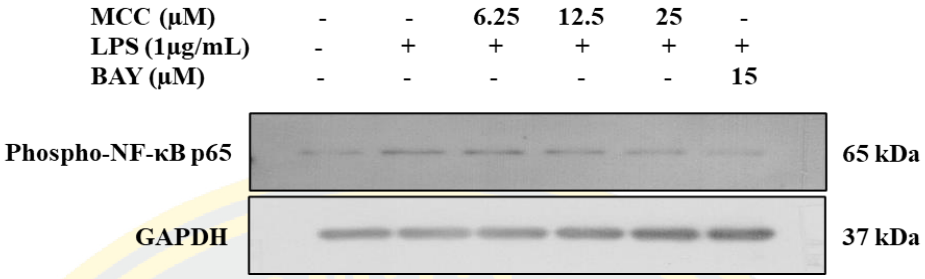

(B)

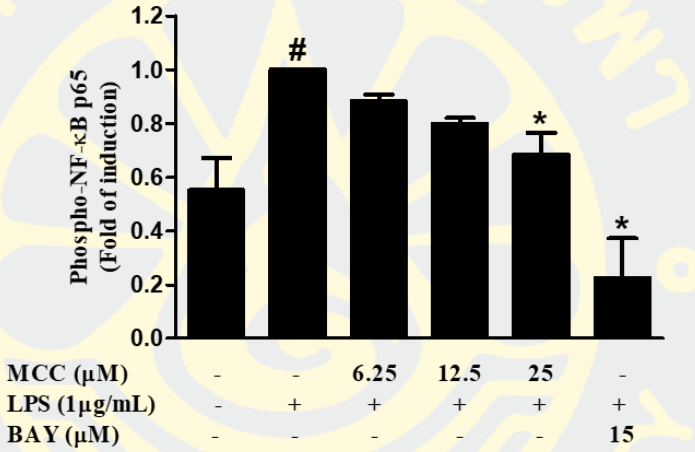

Figure 4-20 Effect of MCC on NF-κB p65 phosphorylation in LPS-stimulated BV2 microglial cells. Cells were pre-treated with MCC at the concentrations of 6.25-25 µM and 15 µM of BAY 11-7082 (BAY) for 1 h before stimulating with 1 µg/mL of LPS for 30 min. Total protein was determined by Western blot analysis (A). Each column shows a mean±SD of densitometric values determined by Image Studio Lite 5.2 Quick Start Guide program and the phospho-NF-κB p65 were normalized with GAPDH (n=3) (B). Data are expressed as a fold change of LPS-stimulated cells. #p<0.05 compared with unstimulated control cells and *p<0.05 compared with LPS-stimulated cells.

(A)

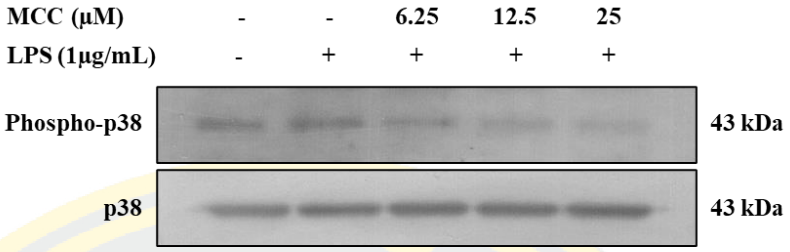

(B)

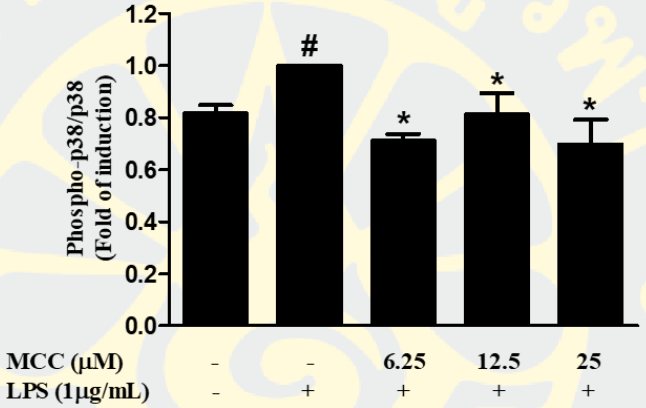

Figure 4-21 Effect of MCC on p38 MAP kinase phosphorylation in LPS-stimulated BV2 microglial cells. Cells were pre-treated with MCC at the concentrations of 6.25-25 µM for 1 h before stimulating with 1 µg/mL LPS for 30 min. Total protein was analyzed for the level of phospho-p38 and p38 by Western blot analysis (A). Each column shows a mean±SD of densitometric values determined by Image Studio Lite 5.2 Quick Start Guide program and the phospho-p38 were normalized with p38 total protein (B). Data are expressed as a fold change of LPS-stimulated cells. #$p<0.05$ compared with unstimulated control cells and *$p<0.05$ compared with LPS-stimulated cells.

(A)

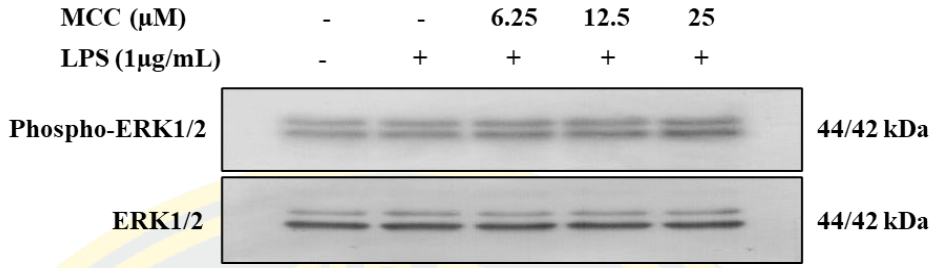

(B)

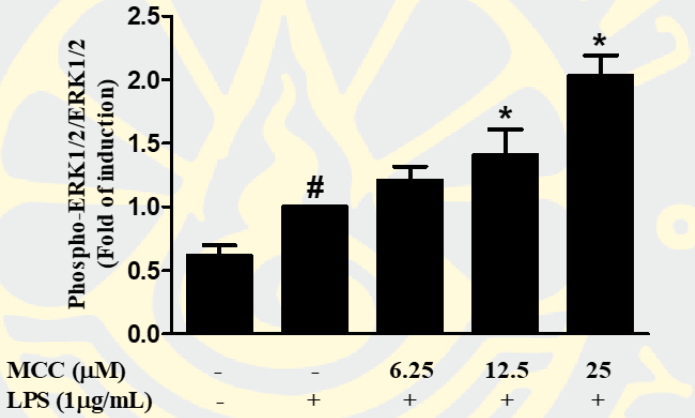

Figure 4-22 Effect of MCC on ERK MAP kinase phosphorylation in LPS-stimulated BV2 microglial cells. Cells were pre-treated with MCC at the concentrations of 6.25-25 µM for 1 h before stimulating with 1 µg/mL LPS for 30 min. Total protein was analyzed for the level of phospho-ERK and ERK by Western blot analysis (A). Each column shows a mean±SD of densitometric values determined by Image Studio Lite 5.2 Quick Start Guide program and the phospho-ERK were normalized with ERK total protein (B). Data are expressed as a fold change of LPS-stimulated cells. #p<0.05 compared with unstimulated control cells and *p<0.05 compared with LPS-stimulated cells.

(A)

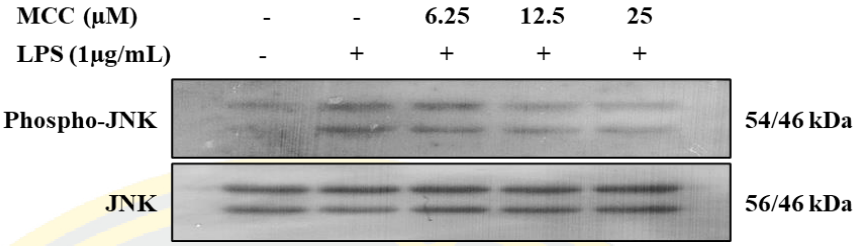

(B)

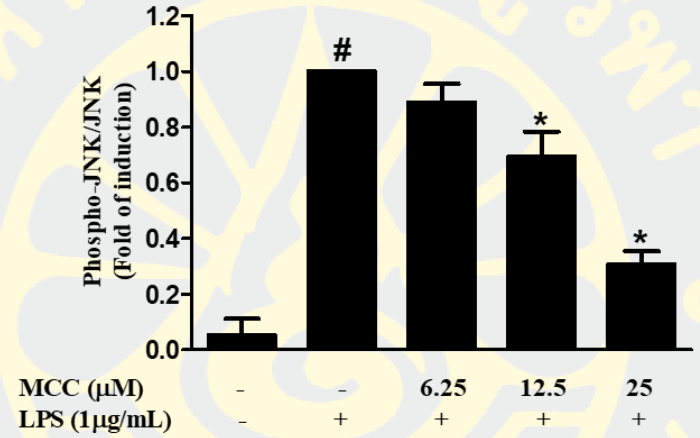

Figure 4-23 Effect of MCC on JNK MAP kinase phosphorylation in LPS-stimulated BV2 microglial cells. Cells were pre-treated with MCC at the concentrations of 6.25-25 µM for 1 h before stimulating with 1 µg/mL LPS for 30 min. Total protein was analyzed for the level of phospho-JNK and JNK by Western blot analysis (A). Each column shows a mean±SD of densitometric values determined by Image Studio Lite 5.2 Quick Start Guide program and the phospho-JNK were normalized with JNK total protein (B). Data are expressed as a fold change of LPS-stimulated cells. #$p<0.05$ compared with unstimulated control cells and *$p<0.05$ compared with LPS-stimulated cells.

CHAPTER 5
DISCUSSION

The primary purpose of this study was to evaluate the anti-inflammatory activity of ethanol extract and a major active compound, MCC from *E. pavieana* rhizomes on microglial cells. Moreover, the molecular mechanisms underlying their anti-inflammatory effect were examined. Microglial cells are CNS-resident immune cells that play crucial roles in neuroinflammatory process (Voet et al., 2018). The activation of microglial cells by stimuli leads to the secretion of pro-inflammatory mediators and cytokines such as NO, PGE_2 and TNF-α (Liu & Hong, 2003; Gao et al., 2017). Nonetheless, overactivation of microglial cells causes the excessive and chronic production of these pro-inflammatory mediators and cytokines, which play a role in the development of neurodegenerative diseases (Block et al., 2007; Chen et al., 2016). In this study, LPS-induced BV2 microglial cells were employed as an *in vitro* neuroinflammatory model. BV2 cells have been shown that the behaviors in cytokine secretion, synaptic plasticity and neuronal networking of BV2 microglial cells are similar to those of primary microglial cells (Sarkar et al., 2018). Moreover, BV2 microglial cells treated with LPS are recognized as a convenient research tool for studying neuroinflammatory mechanisms (He et al., 2018; Sivaprakasam et al., 2019) and has been widely used in many studies to evaluate the potential of anti-inflammatory agents (Wang-Sheng et al., 2017; Wu, Zhong, Yu, & Qi, 2019; Do et al., 2020).

In the previous study, the ethanol extract of *E. pavieana* rhizomes (EPE) has been exerted anti-inflammatory activity in LPS-stimulated RAW 264.7 macrophages by suppression of iNOS expression and NO production (Srisook et al., 2017). EPE also effectively inhibited intracellular ROS production (Srisook et al., 2018) and exerted anti-vascular inflammatory activity in TNF-α-stimulated human endothelial cells (Srisook et al., 2020). However, inhibitory activity on neuroinflammation of EPE remains unknown. In this study, EPE was performed to assess the anti-inflammatory effect in LPS-stimulated BV2 microglial cells. The results demonstrated that EPE strongly reduced the production of NO and PGE_2 in a concentration-

dependent manner. Furthermore, the results of EPE on cell viability shows that EPE at concentration 6.25-100 µg/mL did not significantly altered the viability of cells when compared with unstimulated control cells. This result indicated that the reduction of NO and PGE_2 production were not mediated by the cytotoxicity of EPE.

A large of NO and PGE_2 production in LPS-activated microglial cells is known to be mainly generated by the regulation of iNOS and COX-2, respectively (Lima, Bastos, Limborço-Filho, Fiebich, & de Oliveira, 2012; Dagdeviren, 2017). Since EPE exhibited the inhibitory activity on LPS-stimulated NO and PGE_2 production, the expression levels of iNOS and COX-2 were assessed. The present study showed that EPE decreased LPS-stimulated iNOS and COX-2 in both protein and mRNA expression. This result is coincided with previous study from Srisook et al. (2017) which reported that EPE decreased NO production and inhibited iNOS mRNA and protein expression in LPS-induced RAW 264.7 macrophages. Our findings revealed that the reduction of NO and PGE_2 production by EPE might be mediated via the inhibition of iNOS mRNA and protein expression levels.

Transcription factor NF-κB is a major inflammatory response regulator and widely known to control the activation of inflammatory genes such as iNOS, COX-2 and TNF-α (Mattson, 2005; Sun, 2017; Lim, Kim, Kim, Park, & Jeong, 2018). The NF-κB is activated when cellular stimulation with harmful stimuli such as LPS, triggers the activation of IKK complex. The activated IKK then phosphorylates IκBα on Ser32 and Ser36, mediating its ubiquitination and proteasomal degradation. Simultaneously, the activation of IKK serves to phosphorylate the NF-κB p65 subunit on Ser536 (Buss et al., 2004). This results in freed NF-κB dimer translocation into the cellular nucleus and binding to specific regions on target gene enhancers or promoters to regulate transcription (Jayasooriya et al., 2014; Liu, Zhang, Joo, & Sun, 2017; Dresselhaus & Meffert, 2019). Accordingly, modulation of NF-κB activity is considered as a promising target for the prevention of neurodegenerative diseases. In this study, EPE suppressed the phosphorylation on IκBα and NF-κB p65 subunit. The results indicated that the anti-inflammatory mechanism of EPE in microglial cells was possibly by inactivation of the NF-κB signaling pathway through the suppression on the phosphorylation of IκBα and NF-κB p65 lead to the suppression of iNOS and COX-2 genes transcription. Our finding is in the line with the result from Srisook and

coworker which reported that *E. pavieana* rhizomes suppressed NF-κB activation in LPS-induced RAW 264.7 macrophages (Srisook et al., 2017) and TNF-α-stimulated human endothelial cells (Srisook, Potiprasart, Sarapusit, Park, & Srisook, 2020).

Recently, the active compounds from *E. pavieana* rhizomes was isolated by NO inhibition-guided isolation. MCC is the active compounds isolated from *E. pavieana* rhizomes, which exerted the most effective inhibitory activity on LPS-stimulated NO production in RAW 264.7 macrophages (Srisook et al., 2017). Cumulative studies have shown that MCC exhibit anti-inflammatory activities in LPS-induced RAW 264.7 macrophages (Mankhong et al., 2017; Mankhong et al., 2019) and in TNF-α-stimulated human endothelial cells (Srisook et al., 2020). Also, MCC exhibited in vivo anti-inflammatory response in an acute inflammation rat model (Chiranthanut et al., 2021). Nevertheless, the anti-inflammatory activities of MCC in microglial cells have never been reported. Herein, the anti-inflammatory activity and possible mechanisms involved in LPS-induced BV2 microglial cells were investigated.

The data in Figure 4-11 and 4-14 shows that MCC remarkably decreased LPS-stimulated NO and PGE_2 production in a concentration-dependent manner with an IC_{50} values of 3.32±1.13 μM and 13.32±2.18 μM, respectively. These results are consistent with previous reported by Mankhong et al. (2017 and 2019) which demonstrated the inhibitory activity of MCC on NO and PGE_2 production in LPS-induced RAW 264.7 macrophages. MCC inhibits NO and PGE_2 production in BV2 microglial cells 4.2 folds and 2.5 folds more than that of RAW 264.7 macrophage cells, respectively. Furthermore, the results in Figure 4-12 and 4-13 shows that MCC significantly declined LPS-stimulated iNOS in both mRNA and protein expression. Hence, the reduction of NO production by MCC is due to the suppression of iNOS protein and mRNA expression. Intriguingly, the data in Figure 4-15 and 4-16 showed that the expression of COX-2 mRNA and protein was significantly inhibited by MCC at a concentration of 25 μM while the inhibitory effect of MCC on LPS-induced PGE_2 production was observed at 6.25-25 μM (Figure 4-14). It should be observed that the degree of PGE_2 suppression by MCC was higher than COX-2 expression. PGE_2 production is not only by modulation of COX-2 expression, but also be produced by modulation of COX-2 activity (Kalinski, 2012; Mankhong et al., 2019). Thus, the

suppression of PGE_2 production by MCC could possibly not only inhibit the expression of COX-2, but may also inhibit its activity. However, further studies are required to clear up this point.

Cytokines are small secreted proteins that have been reported to play a crucial role in the neuroinflammatory process and neurodegenerative diseases (Smith, Das, Ray, & Banik, 2012). TNF-α is a major cytokine produced by activated microglial cells that aids in immune response (Probert, 2015). TNF-α overproduction causes excessive inflammation, which is an etiologic factor in the development of neurodegenerative diseases (Olmos & Lladó, 2014; Jung, Tweedie, Scerba, & Greig, 2019). In this study, MCC significantly reduced LPS-stimulated TNF-α production. Also, the expression of TNF-α mRNA was suppressed by MCC (Figure 4-18). Our findings indicated that MCC inhibits LPS-stimulated TNF-α production by attenuating its transcription level. Accordingly, these results confirmed that MCC exhibits anti-inflammatory activity on LPS-induced BV2 microglial cells through reducing pro-inflammatory mediators and cytokines. Moreover, these findings are in line with the previous observation on LPS-stimulated RAW264.7 macrophages (Mankhong et al., 2019).

It was also found that MCC significantly arrested the NF-κB activation by suppression of the phosphorylation on IκBα and NF-κB p65 in BV2 microglial cells. This result is in the line with the result from Mankhong et al. (2019) which reported that MCC exerted anti-inflammatory effect on LPS-stimulated RAW264.7 macrophages by blocking the activation of NF-κB via suppression of IκBα phosphorylation and nuclear translocation of NF-κB p65 (Mankhong et al., 2019). Therefore, our findings suggested that the anti-inflammatory activity of MCC in BV2 microglial cells through suppression on the phosphorylation IκBα and NF-κB p65 which leads to attenuating NF-κB nuclear translocation.

MAPKs are an evolutionally conserved family of signaling molecules related in the regulation of inflammatory responses. The phosphorylation of MAPKs, which includes JNK, p38 and ERK1/2, can induce a variety of transcription factors resulting in pro-inflammatory mediators and cytokines expression upon stimulus condition (Kim & Choi, 2010). Thus, MCC was investigated whether it regulate MAPKs phosphorylation. In LPS-induced BV2 microglial cells, MCC exhibited

significantly inhibition of p38 and JNK phosphorylation. Noticeably, MCC obviously enhanced the phosphorylation of ERK1/2. Previous studies have been reported that agents that exert neuroprotective activity could inhibit the phosphorylation of EKK1/2 (Olajide, Aderogba, & Fiebich, 2013; Wang et al., 2015; Jo et al., 2019; Do et al., 2020). However, our findings are consistent with previous findings from Chen and coworkers, which reported that scutellarin suppressed p38 and JNK phosphorylation but increased ERK1/2 phosphorylation in LPS-activated BV2 microglial cells (Chen et al., 2020). Based on these results, the inhibitory activity of MCC on NO, PGE_2 and TNF-α was, at least in part, mediated dependently of MAPKs pathway. Our finding is not consistent with previous findings in RAW264.7 macrophage cells, which demonstrated that anti-inflammatory activity of MCC was mediated independently of MAPKs activation but mediated by inactivation of NF-κB and AP-1 transcription factors through downregulation of the PI3K/Akt signaling pathway (Mankhong et al., 2019). This contention may be owing to different cell types which respond to agonist in different downstream signaling pathways.

In conclusion, our results in this study demonstrated that EPE exerts an anti-inflammatory activity in LPS-stimulated BV2 microglial cells via suppressing the expression of iNOS and COX-2 which may be occurring via inactivation of NF-κB signaling pathway. Moreover, MCC exerted an inhibitory activity on pro-inflammatory mediators and cytokine. The mechanism underlying inhibitory effect of MCC was probably mediated through suppressing the activation of NF-κB and MAPKs signaling pathway. Nevertheless, further studies are imperative to clarify the exact molecular mechanism of MCC. The obtained data suggests that *E. pavieana* rhizome and MCC might be useful in the development as a dietary supplement or an ingredient in functional food for preventing neurodegenerative diseases.

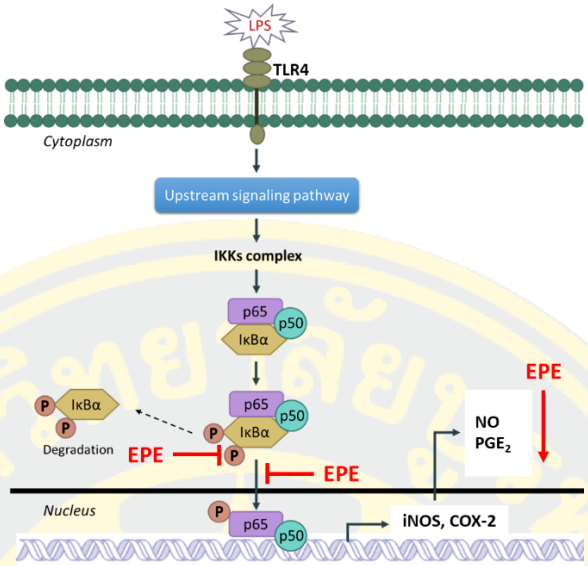

Figure 5-1 A schematic diagram of the mechanism proposed for anti-inflammatory action of EPE in LPS-stimulated BV2 microglial cells. EPE inhibited pro-inflammatory mediators in LPS-stimulated BV2 microglial cells through suppression of the activation of NF-κB signaling pathway.

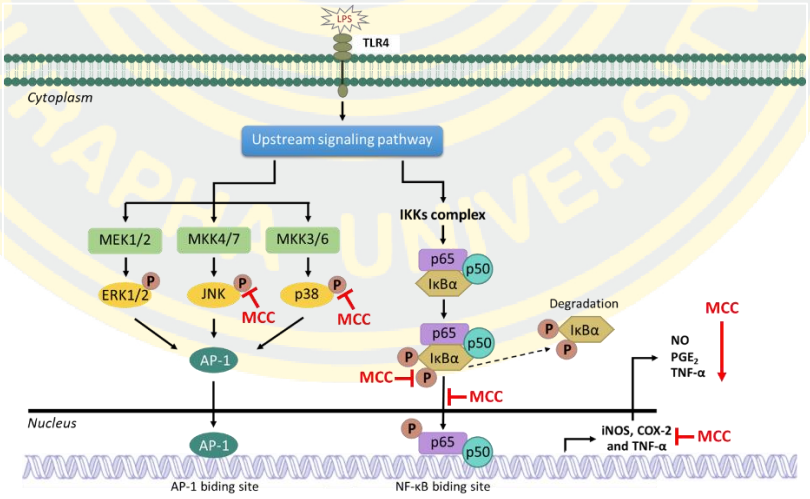

Figure 5-2 A schematic diagram of the mechanism proposed for anti-inflammatory action of MCC in LPS-stimulated BV2 microglial cells. MCC inhibited pro-inflammatory mediators and cytokine in LPS-stimulated BV2 microglial cells through suppression the activation of NF-κB and MAPKs signaling pathway.

REFFERENCES

Ali, T. B., Schleret, T. R., Reilly, B. M., Chen, W. Y., & Abagyan, R. (2015). Adverse effects of cholinesterase inhibitors in dementia, according to the pharmacovigilance databases of the United-States and Canada. *PLoS One, 10*(12), e0144337.

Amor, S., Peferoen, L. A., Vogel, D. Y., Breur, M., van der Valk, P., Baker, D., & van Noort, J. M. (2014). Inflammation in neurodegenerative diseases–an update. *Immunology, 142*(2), 151-166.

Amor, S., Puentes, F., Baker, D., & Van Der Valk, P. (2010). Inflammation in neurodegenerative diseases. *Immunology, 129*(2), 154-169.

Bazan, N. G., Halabi, A., Ertel, M., & Petasis, N. A. (2012). Neuroinflammation. *In Basic Neurochemistry* (pp. 610-620). Academic Press.

Biology Blog. (2016). Western Blot. Retrieved from http://bioisnotdifficult.blogspot.com/2016/07/western-blotting.html

Birks, J. S. (2006). Cholinesterase inhibitors for Alzheimer's disease. *Cochrane Database of Systematic Reviews,* (1).

Block, M. L., & Hong, J. S. (2005). Microglia and inflammation-mediated neurodegeneration: multiple triggers with a common mechanism. *Progress in Neurobiology, 76*(2), 77-98.

Block, M. L., Zecca, L., & Hong, J. S. (2007). Microglia-mediated neurotoxicity: uncovering the molecular mechanisms. *Nature Reviews Neuroscience, 8*(1), 57-69.

Brás, J. P., Bravo, J., Freitas, J., Barbosa, M. A., Santos, S. G., Summavielle, T., & Almeida, M. I. (2020). TNF-alpha-induced microglia activation requires miR-342: impact on NF-kB signaling and neurotoxicity. *Cell death & Disease, 11*(6), 1-15.

Bryan, N. S., & Grisham, M. B. (2007). Methods to detect nitric oxide and its metabolites in biological samples. *Free Radical Biology and Medicine, 43*(5), 645-657.

Buss, H., Dörrie, A., Schmitz, M. L., Hoffmann, E., Resch, K., & Kracht, M. (2004). Constitutive and interleukin-1-inducible phosphorylation of p65 NF-κB at serine 536 is mediated by multiple protein kinases including IκB kinase (IKK)-α, IKKβ, IKKϵ, TRAF family member-associated (TANK)-binding kinase 1 (TBK1), and an unknown kinase and couples p65 to TATA-binding protein-associated factor II31-mediated interleukin-8 transcription. *Journal of Biological Chemistry, 279*(53), 55633-55643.

Bustin, S. A., & Mueller, R. (2005). Real-time reverse transcription PCR (qRT-PCR) and its potential use in clinical diagnosis. *Clinical Science, 109*(4), 365-379.

Calabrese, V., Mancuso, C., Calvani, M., Rizzarelli, E., Butterfield, D. A., & Stella, A. M. G. (2007). Nitric oxide in the central nervous system: neuroprotection versus neurotoxicity. *Nature Reviews Neuroscience, 8*(10), 766.

Cascione, M., De Matteis, V., Leporatti, S., & Rinaldi, R. (2020). The New Frontiers in Neurodegenerative Diseases Treatment: Liposomal-Based Strategies. *Frontiers in Bioengineering and Biotechnology, 8*, 1166.

Chen, H. L., Jia, W. J., Li, H. E., Han, H., Li, F., Li, J. J., ... & Wu, C. Y. (2020). Scutellarin exerts anti-inflammatory effects in activated microglia/brain macrophage in cerebral ischemia and in activated BV-2 microglia through regulation of MAPKs signaling pathway. *Neuromolecular Medicine, 22*(2), 264-277.

Chen, W. W., Zhang, X. I. A., & Huang, W. J. (2016). Role of neuroinflammation in neurodegenerative diseases. *Molecular Medicine Reports, 13*(4), 3391-3396.

Chiranthanut, N., Lertprasertsuke, N., Srisook, E., & Srisook, K. (2021). Anti-inflammatory effect and acute oral toxicity of 4-methoxycinnamyl *p*-coumarate isolated from *Etlingera pavieana* rhizomes in animal models. *Journal of Applied Pharmaceutical Science, 11*(10), 024-028.

Cuenda, A., & Rousseau, S. (2007). p38 MAP-kinases pathway regulation, function and role in human diseases. *Biochimica et Biophysica Acta (BBA)-Molecular Cell Research, 1773*(8), 1358-1375.

Dagdeviren, M. (2017). Role of Nitric Oxide Synthase in Normal Brain Function and Pathophysiology of Neural Diseases. *Nitric Oxide Synthase: Simple Enzyme-Complex Roles, 37*.

Daniels, J. W. (2012). Current PCR Methods. Retrieved from http://www.labome.com /method/Current-PCR-Methods.html

Department of Mental Health. (2018). Retrieved from http://www.prdmh.com/

DiSabato, D. J., Quan, N., & Godbout, J. P. (2016). Neuroinflammation: the devil is in the details. *Journal of Neurochemistry, 139,* 136-153.

Do, H. T. T., Bui, B. P., Sim, S., Jung, J. K., Lee, H., & Cho, J. (2020). Anti-Inflammatory and Anti-Migratory Activities of Isoquinoline-1-Carboxamide Derivatives in LPS-Treated BV2 Microglial Cells via Inhibition of MAPKs/NF-κB Pathway. *International Journal of Molecular Sciences, 21*(7), 2319.

Dresselhaus, E. C., & Meffert, M. K. (2019). Cellular specificity of NF-κB function in the nervous system. *Frontiers in Immunology, 10,* 1043.

Durães, F., Pinto, M., & Sousa, E. (2018). Old drugs as new treatments for neurodegenerative diseases. *Pharmaceuticals, 11*(2), 44.

Fitzpatrick, F. A. (2004). Cyclooxygenase enzymes: regulation and function. *Current Pharmaceutical Design, 10*(6), 577-588.

Förstermann, U., & Sessa, W. C. (2011). Nitric oxide synthases: regulation and function. *European Heart Journal, 33*(7), 829-837.

Frakes, A. E., Ferraiuolo, L., Haidet-Phillips, A. M., Schmelzer, L., Braun, L., Miranda, C. J., ... & Kaspar, B. K. (2014). Microglia induce motor neuron death via the classical NF-κB pathway in amyotrophic lateral sclerosis. *Neuron, 81*(5), 1009-1023.

Gan, S. D., & Patel, K. R. (2013). Enzyme immunoassay and enzyme-linked immunosorbent assay. *J Invest Dermatol, 133*(9), e12.

Gandhi, K. R., & Saadabadi, A. (2020). Levodopa (l-dopa). *StatPearls*.

Gao, H. M., & Hong, J. S. (2008). Why neurodegenerative diseases are progressive: uncontrolled inflammation drives disease progression. *Trends in Immunology, 29*(8), 357-365.

Gao, H. M., Tu, D., Gao, Y., Liu, Q., Yang, R., Liu, Y., ... & Hong, J. S. (2017). Roles of microglia in inflammation-mediated neurodegeneration: models, mechanisms, and therapeutic interventions for Parkinson's disease. *In Advances in Neurotoxicology* (Vol. 1, pp. 185-209). Academic Press.

Ginhoux, F., Greter, M., Leboeuf, M., Nandi, S., See, P., Gokhan, S., ... & Merad, M. (2010). Fate mapping analysis reveals that adult microglia derive from primitive macrophages. *Science, 330*(6005), 841-845.

Giulietti, A., Overbergh, L., Valckx, D., Decallonne, B., Bouillon, R., & Mathieu, C. (2001). An overview of real-time quantitative PCR: applications to quantify cytokine gene expression. *Methods, 25*(4), 386-401.

Glass, C. K., Saijo, K., Winner, B., Marchetto, M. C., & Gage, F. H. (2010). Mechanisms underlying inflammation in neurodegeneration. *Cell, 140*(6), 918-934.

Grewal, S. S., York, R. D., & Stork, P. J. (1999). Extracellular-signal-regulated kinase signaling in neurons. *Current Opinion in Neurobiology, 9*(5), 544-553.

Hayden, M. S., & Ghosh, S. (2008). Shared principles in NF-κB signaling. *Cell, 132*(3), 344-362.

He, Y., Yao, X., Taylor, N., Bai, Y., Lovenberg, T., & Bhattacharya, A. (2018). RNA sequencing analysis reveals quiescent microglia isolation methods from postnatal mouse brains and limitations of BV2 cells. *Journal of Neuroinflammation, 15*(1), 1-13.

Hein, A. M., & O'Banion, M. K. (2009). Neuroinflammation and memory: the role of prostaglandins. *Molecular Neurobiology, 40*(1), 15-32.

Heneka, M. T., Carson, M. J., El Khoury, J., Landreth, G. E., Brosseron, F., Feinstein, D. L., ... & Herrup, K. (2015). Neuroinflammation in Alzheimer's disease. *The LancetNeurology, 14*(4), 388-405.

Hoesel, B., & Schmid, J. A. (2013). The complexity of NF-κB signaling in inflammation and cancer. *Molecular Cancer, 12*(1), 86.

Iawsipo, P., Srisook, E., Ponglikitmongkol, M., Somwang, T., & Singaed, O. (2018). Cytotoxic effects of *Etlingera pavieana* rhizome on various cancer cells and identification of a potential anti-tumor component. *Journal of Food Biochemistry, 42*(4), e12540.

Jayasooriya, R. G. P. T., Lee, K. T., Lee, H. J., Choi, Y. H., Jeong, J. W., & Kim, G. Y. (2014). Anti-inflammatory effects of β-hydroxyisovalerylshikonin in BV2 microglia are mediated through suppression of the PI3K/Akt/NF-kB pathway and activation of the Nrf2/HO-1 pathway. *Food and Chemical Toxicology, 65*, 82-89.

Jo, S. H., Kim, M. E., Cho, J. H., Lee, Y., Lee, J., Park, Y. D., & Lee, J. S. (2019). Hesperetin inhibits neuroinflammation on microglia by suppressing inflammatory cytokines and MAPK pathways. *Archives of pharmacal research, 42*(8), 695-703.

Jost, P. J., & Ruland, J. (2007). Aberrant NF-κB signaling in lymphoma: mechanisms, consequences, and therapeutic implications. *Blood, 109*(7), 2700-2707.

Jung, Y. J., Tweedie, D., Scerba, M. T., & Greig, N. H. (2019). Neuroinflammation as a factor of neurodegenerative disease: thalidomide analogs as treatments. *Frontiers in Cell and Developmental Biology, 7*, 313.

Kalinski, P. (2012). Regulation of immune responses by prostaglandin E_2. *The Journal of Immunology*, *188*(1), 21-28.

Keshet, Y., & Seger, R. (2010). The MAP kinase signaling cascades: a system of hundreds of components regulates a diverse array of physiological functions. In MAP Kinase Signaling Protocols (pp. 3-38). *Humana Press, Totowa, NJ.*

Kiaei, M. (2013). New hopes and challenges for treatment of neurodegenerative disorders: Great opportunities for young neuroscientists. *Basic and Clinical Neuroscience, 4*(1), 3.

Kim, E. K., & Choi, E. J. (2010). Pathological roles of MAPK signaling pathways in human diseases. *Biochimica et Biophysica Acta (BBA)-Molecular Basis of Disease, 1802*(4), 396-405.

Kopitar-Jerala, N. (2015). Innate immune response in brain, NF-kappa B signaling and cystatins. *Frontiers in Molecular Neuroscience,* 8, 73.

Kuno, R., Wang, J., Kawanokuchi, J., Takeuchi, H., Mizuno, T., & Suzumura, A. (2005). Autocrine activation of microglia by tumor necrosis factor-α. *Journal of Neuroimmunology, 162*(1-2), 89-96.

Li, L., Zhao, G. D., Shi, Z., Qi, L. L., Zhou, L. Y., & Fu, Z. X. (2016). The Ras/Raf/

MEK/ERK signaling pathway and its role in the occurrence and development of HCC. *Oncology Letters, 12*(5), 3045-3050.

Lim, H. S., Kim, Y. J., Kim, B. Y., Park, G., & Jeong, S. J. (2018). The anti-neuroinflammatory activity of tectorigenin pretreatment via downregulated NF-κB and ERK/JNK pathways in BV-2 microglial and microglia inactivation in mice with lipopolysaccharide. *Frontiers in Pharmacology, 9*, 462.

Lima, I. V. D. A., Bastos, L. F. S., Limborço-Filho, M., Fiebich, B. L., & de Oliveira, A. C. P. (2012). Role of prostaglandins in neuroinflammatory neurodegenerative diseases. *Mediators of Inflammation. 2012.*

Liu, B., & Hong, J. S. (2003). Role of microglia in inflammation-mediated neurodegenerative diseases: mechanisms and strategies for therapeutic intervention. *Journal of Pharmacology and Experimental Therapeutics, 304*(1), 1-7.

Liu, T., Zhang, L., Joo, D., & Sun, S. C. (2017). NF-κB signaling in inflammation. *Signal Transduction and Targeted Therapy, 2*(1), 1-9.

Lull, M. E., & Block, M. L. (2010). Microglial activation and chronic neurodegeneration. *Neurotherapeutics, 7*(4), 354-365.

Mahmood, T., & Yang, P. C. (2012). Western blot: technique, theory, and trouble shooting. *North American Journal of Medical Sciences, 4*(9), 429.

Mankhong, S., Iawsipo, P., Srisook, E., & Srisook, K. (2019). 4-methoxycinnamyl p-coumarate isolated from *Etlingera pavieana* rhizomes inhibits inflammatory response via suppression of NF-κB, Akt and AP-1 signaling in LPS-stimulated RAW 264.7 macrophages. *Phytomedicine, 54*, 89-97.

Mankhong, S., Srisook, E., & Srisook, K. (2017). Anti-inflammatory activity of 4-methoxycinnamyl p-coumarate isolated from *Etlingera pavieana* rhizomes in lipopolysaccharide-induced macrophages. NU. *International Journal of Science, 14*(2), 58-66.

MBL Life science. (2019). The principle and method of ELISA. Retrieved from http://ruo.mbl.co.jp/bio/e/support/method/elisa.html

Milatovic, D., Zaja-Milatovic, S., Breyer, R. M., Aschner, M., & Montine, T. J. (2017). Neuroinflammation and oxidative injury in developmental

neurotoxicity. *In Reproductive and Developmental Toxicology* (pp. 1051-1061). Academic Press.

Morales, I., Guzmán-Martínez, L., Cerda-Troncoso, C., Farías, G. A., & Maccioni, R. B. (2014). Neuroinflammation in the pathogenesis of Alzheimer's disease. A rational framework for the search of novel therapeutic approaches. *Frontiers in Cellular Neuroscience, 8*, 112.

Mattson, M. P. (2005). NF-κB in the survival and plasticity of neurons. *Neurochemical Research, 30*(6), 883-893.

Neniskyte, U., Vilalta, A., & Brown, G. C. (2014). Tumour necrosis factor alpha-induced neuronal loss is mediated by microglial phagocytosis. *FEBS Letters, 588*(17), 2952-2956.

National Institute of Environmental Health Sciences. (2021). Neurodegenerative Diseases. Available from: http://www.niehs.nih.gov/research/supported /health/neurodegenerative/index.cfm.

Olajide, O. A., Aderogba, M. A., & Fiebich, B. L. (2013). Mechanisms of anti-inflammatory property of *Anacardium occidentale* stem bark: inhibition of NF-κB and MAPK signaling in the microglia. *Journal of Ethnopharmacology, 145*(1), 42-49.

Olmos, G., & Lladó, J. (2014). Tumor necrosis factor alpha: a link between neuroinflammation and excitotoxicity. *Mediators of inflammation, 2014*.

Ott, L. W., Resing, K. A., Sizemore, A. W., Heyen, J. W., Cocklin, R. R., Pedrick, N. M., ... & Harrington, M. A. (2007). Tumor necrosis factor-α-and interleukin-1 induced cellular responses: Coupling proteomic and genomic information. *Journal of Proteome Research, 6*(6), 2176-2185.

Poddar, M. K., Chakraborty, A., & Banerjee, S. (2021). Neurodegeneration: Diagnosis, Prevention, and Therapy. *In Oxidoreductase*. IntechOpen.

Pomary, P. K. (2016). Exploring differences in protein metabolites in cerebrospinal fluid from patients with Alzheimer's disease, frontotemporal dementia or amyotrophic lateral sclerosis: a pilot study (Master's thesis, NTNU).

Poulsen, A. D., & Phonsena, P. (2017). Morphological variation and distribution of the useful ginger *Etlingera pavieana* (Zingiberaceae). Nordic Journal of Botany, 35(4), 467-475.

Probert, L. (2015). TNF and its receptors in the CNS: The essential, the desirable and the deleterious effects. *Neuroscience*, *302*, 2-22.

Promega. (2009). Griess Reagent System. Retrieved from http://ruo.mbl.co.jp/bio/e/support/method/elisa.html

Ramos, J. W. (2008). The regulation of extracellular signal-regulated kinase (ERK) in mammalian cells. *The International Journal of Biochemistry & Cell Biology*, *40*(12), 2707-2719.

Ricciotti, E., & FitzGerald, G. A. (2011). Prostaglandins and inflammation. *Arteriosclerosis, Thrombosis, and Vascular Biology*, *31*(5), 986-1000.

Rose, B. A., Force, T., & Wang, Y. (2010). Mitogen-activated protein kinase signaling in the heart: angels versus demons in a heart-breaking tale. *Physiological Reviews*, *90*(4), 1507-1546.

Saavedra-López, E., Casanova, P.V., CribaroC.Barcia, G.P. (2016). Neuroinflammation in Movement Disorders. Handbook of Behavioral Neuroscience, 24, 771-782.

Sarkar, S., Malovic, E., Sarda, D., Lawana, V., Rokad, D., Jin, H., ... & Kanthasamy, A. G. (2018). Characterization and comparative analysis of a new mouse microglial cell model for studying neuroinflammatory mechanisms during neurotoxic insults. *Neurotoxicology*, *67*, 129-140.

Shaul, Y. D., & Seger, R. (2007). The MEK/ERK cascade: from signaling specificity to diverse functions. Biochimica et Biophysica Acta (BBA)-Molecular Cell Research, 1773(8), 1213-1226.

Sivaprakasam, G., Ganesan, P., Muniandy, K., Park, S. Y., Cho, D. Y., Kim, J. S., ... & Choi, D. K. (2019). Attenuation of lipopolysaccharide-induced neuroinflammatory events in BV-2 microglial cells by *Moringa oleifera* leaf extract. *Asian Pacific Journal of Tropical Biomedicine*, *9*(3), 109.

Smith, J. A., Das, A., Ray, S. K., & Banik, N. L. (2012). Role of pro-inflammatory cytokines released from microglia in neurodegenerative diseases. Brain Research Bulletin, 87(1), 10-20.

Srisook, E., Palachot, M., Mankhong, S., & Srisook, K. (2017). Anti-inflammatory effect of *Etlingera pavieana* (Pierre ex Gagnep.) RM Sm. rhizomal extract and its phenolic compounds in lipopolysaccharide-stimulated macrophages.

Pharmacognosy Magazine, 13(Suppl 2), S230.

Srisook, K., Potiprasart, K., Sarapusit, S., Park, C. S., & Srisook, E. (2020). *Etlingera pavieana* extract attenuates TNF-α induced vascular adhesion molecule expression in human endothelial cells through NF-κB and Akt/JNK pathways. *Inflammopharmacology, 28*(6), 1649-1662.

Srisook, K., Srisook, E., Nachaiyo, W., Chan-In, M., Thongbai, J., Wongyoo, K., ... & Watcharanawee, K. (2015). Bioassay-guided isolation and mechanistic action of anti-inflammatory agents from *Clerodendrum inerme* leaves. *Journal of Ethnopharmacology, 165*, 94-102.

Srisook, K., Udompong, S., Sawai, P., & Thongyen, T. (2018). *Etlingera pavieana* rhizome extract decreases oxidative stress and activates eNOS activity via stimulation of Akt phosphorylation in human endothelial cells. *Naresuan Phayao Journal, 11*(1), 23-28.

Sun, S. C. (2011). Non-canonical NF-κB signaling pathway. *Cell Research, 21*(1), 71.

Sun, S. C. (2017). The non-canonical NF-κB pathway in immunity and inflammation. *Nature reviews Immunology, 17*(9), 545-558.

Tachai, S., & Nuntawong, N. (2016). Uncommon secondary metabolites from *Etlingera pavieana* rhizomes. *Natural Product Research, 30*(19), 2215-2219.

Tansey, M. G., McCoy, M. K., & Frank-Cannon, T. C. (2007). Neuroinflammatory mechanisms in Parkinson's disease: potential environmental triggers, pathways, and targets for early therapeutic intervention. *Experimental Neurology, 208*(1), 1-25.

Voet, S., Prinz, M., & van Loo, G. (2018). Microglia in central nervous system inflammation and multiple sclerosis pathology. *Trends in Molecular Medicine. 25*(2), 112-123.

Wang, H. Y., Wang, H., Wang, J. H., Wang, Q., Ma, Q. F., & Chen, Y. Y. (2015). Protocatechuic acid inhibits inflammatory responses in LPS-stimulated BV2 microglia via NF-κB and MAPKs signaling pathways. *Neurochemical Research, 40*(8), 1655-1660.

Wang, M. J., Huang, H. Y., Chen, W. F., Chang, H. F., & Kuo, J. S. (2010). Glycogen synthase kinase-3β inactivation inhibits tumor necrosis factor-α production

in microglia by modulating nuclear factor κB and MLK3/JNK signaling cascades. *Journal of Neuroinflammation, 7*(1), 1-18.

Wang-Sheng, C., Jie, A., Jian-Jun, L., Lan, H., Zeng-Bao, X., & Chang-Qing, L. (2017). Piperine attenuates lipopolysaccharide (LPS)-induced inflammatory responses in BV2 microglia. *International Immunopharmacology, 42*, 44-48.

Wang, W. Y., Tan, M. S., Yu, J. T., & Tan, L. (2015). Role of pro-inflammatory cytokines released from microglia in Alzheimer's disease. *Annals of Translational Medicine, 3*(10).

World Health Organization. Dementia. (2020). Available from: https://www.who.int/news-room/fact-sheets/detail/dementia.

Wu, Y., Zhong, L., Yu, Z., & Qi, J. (2019). Anti-neuroinflammatory effects of tannic acid against lipopolysaccharide-induced BV2 microglial cells via inhibition of NF-κB activation. *Drug Development Research, 80*(2), 262-268.

Zhou, L., & Zhu, D. Y. (2009). Neuronal nitric oxide synthase: structure, subcellular localization, regulation, and clinical implications. *Nitric Oxide, 20*(4), 223-230.

APPENDIXS

APPENDIX A

CULTURE MEDIA AND SOLUTIONS

1. Dulbecco's modified Eagle media (DMEM) with phenol red

DMEM powder (Gibco, USA.; 13.5 g) and 3.7 g of $NaHCO_3$ were dissolved in 900 mL of sterile water for injection. The pH of the solution was adjusted to 7.1-7.2 by adding concentrated of HCl. Then, 10 mL of the antibiotic Penicillin-Streptomycin was added to the solution. The solution was made to a volume of 1,000 mL with sterile water for injection. After that, the solution was sterilized by filter sterilization with membrane (pore size 0.22 µm) and stored in a refrigerator at 4°C.

2. Dulbecco's modified Eagle media (DMEM) with phenol red and 10% heat-inactivated fetal bovine serum (FBS)

DMEM powder (Gibco, USA.; 13.5 g) and 3.7 g of $NaHCO_3$ were dissolved in 800 mL of sterile water for injection. Then, the pH of the solution was adjusted to 7.1-7.2 by adding concentrated HCl. After that, 10 mL of the antibiotic Penicillin-Streptomycin was added to the solution. The solution was made up to a volume of 900 mL with sterile water for injection. The solution was sterilized by filter sterilization with membrane (pore size 0.22 µm). Lastly, 100 ml of heat-inactivated FBS was added into the solution and stored in a refrigerator at 4°C.

3. Dulbecco's modified Eagle medium (DMEM) without phenol red

DMEM powder (Sigma Aldrich, USA.; 10 g), 3.7 g of $NaHCO_3$ and 3.5 g of D-glucose were dissolved in 900 mL of sterile water for injection. Then, the pH of the solution was adjusted to 7.1-7.2 by adding concentrated HCl. After that, 10 mL of the antibiotic Penicillin-Streptomycin was added to the solution. The solution was made to a volume of 1,000 mL with sterile water for injection. Lastly, the solution was sterilized by filter sterilization with membrane (pore size 0.22 µm) and stored in a refrigerator at 4°C.

3. Hank's balance salt solution (HBSS)

0.4 g of KCl, 0.06 g of KH_2PO_4, 8 g of Na_2HPO_4, 1 g of glucose and 0.35 g of $NaHCO_3$ were dissolved in 900 mL of sterile water for injection. After that, the pH of the solution was adjusted to 7.1-7.2 by adding concentrated of HCl and making the

volume up to 1,000 mL with sterile water for injection. Then, 10 mL of Penicillin (100 U/mL) and Streptomycin (100 µg/mL) were added into the solution and sterile by filter sterilization with membrane (pore size 0.22 µm). The solution was stored in a refrigerator at 4°C.

4. 1x Phosphate-Buffer Saline (PBS)

8 g of NaCl, 0.2 g of KCl, 0.24 g of KH_2PO_4 and 1.44 g of Na_2HPO_4 were dissolved in 900 mL of sterile water for injection. After that, the pH of the solution was adjusted to 7.4 and made up volume to 1,000 mL with sterile water for injection. The solution was sterilized by sterilization with membrane (pore size 0.22 µm) and autoclave. The solution was stored in a refrigerator at 4 °C.

5. Thiazolyl Blue Tetrazolium Bromide (MTT) solution (5 mg/mL)

25 mg of MTT was dissolved in 5 mL of 1x PBS and the solution was sterilized by sterilization with a membrane (pore size 0.22 µm). Then, the MTT solution was aliquoted into a 1.5 mL tube and stored in a refrigerator at -20 °C.

6. Griess reagent (10 mL)

0.1 g of Sulfanilamide, 0.01 g of N-napthylene-diamide-chloride or N-(1-napthyl)-ethylenediamine and 0.5 mL of *O*-phosphoric acid were dissolved in 9.5 ml of distilled water. The solution was aliquoted into a 1.5 mL tube and stored in a refrigerator at -20 °C.

APPENDIX B

ELECTROPHORESIS AND BLOTTING SOLUTION

1. 30% (w/v) Monomer solution

29.2 g of acrylamide and 0.8 g of *Bis*-acrylamide were dissolved in distilled water for 100 mL. The solution was sterile by filter sterilization and stored at 4 °C with light protection.

2. 4X separating gel buffer

45.4 g of Tris base (2-hydroxymethyl-2-methyl-1,3-propanediol) was dissolved in distilled water with a volume of 200 mL. The solution was then mixed and the pH was adjusted to 8.8. Lastly, the volume was made up to 250 mL with distilled water and stored at 4 °C.

3. 4X stacking gel buffer

0.6 g of Tris base (2-hydroxymethyl-2-methyl-1,3-propanediol) was dissolved in 80 mL of distilled water. The solution was then mixed with distilled water and adjusted the pH to 6.8. Lastly, the volume is made up to 100 mL before being stored at 4 °C.

4. 10% (w/v) Sodium dodecyl sulfate (SDS)

10 g of SDS dissolved in 10 mL of distilled water. Then, the solution was sterile by filter sterilization and stored at room temperature.

5. 10% (w/v) Ammoniumpersulfate (APS)

0.5 g of APS was dissolved in 10 mL of distilled water. The solution was aliquoted and stored at -20 °C.

6. 10X Tris-glycine running buffer

30.3 g of Tris, 144.2 g of glycine and 10 g of SDS were dissolved in 1000 mL of distilled water and stored at room temperature.

7. Transfer buffer

3.03 g of Tris base and 14.42 g of glycine were dissolved in 850 mL of distilled water, mixed, and 100 mL of methanol were added. The solution was made up to a volume of 1000 mL with distilled water and stored at room temperature.

8. Tris buffer saline (TBS)

5 ml of 2 M Tris-HCl and 37.5 ml of 4 M NaCl were dissolved in distilled water. The solution was made up of 1000 mL of distilled water and stored at room temperature.

9. Tris Buffer Saline with Tween 20 (TBS-T)

1 mL of Tween® 20 was added to 1000 mL of TBS. Then, the solution was mixed and stored at room temperature.

10. Blocking solution (5% skimmed milk)

5 g of non-fat dried milk was dissolved with 100 mL of TBS-T.

11. RIPA protein lysis buffer

15 mL of 1 M Tris-HCl pH 7.4, 3.75 mL of NaCl, 1 mL of o.5 M of EGTA, 1 mL of 10% (w/v) SDS, 5 mL of 20% (w/v) Sodium deoxycholate and 10 mL of 10% (v/v Nodiet P-40 were mixed and made a volume of 100 mL with distilled water. The solution was sterilized by autoclave and stored at 4 °C.

12. RIPA protein lysis buffer for iNOS and COX-2 protein

10 µL of 1 mM of DTT and 10 µL of 100X protease inhibitor (Thermo Scientific, USA.) were mixed in 980 µL of RIPA protein lysis buffer.

13. RIPA protein lysis buffer for NF-κB and MAPKs protein extraction

10 µL of 1 mM of DTT and 10 µL of 100X protease inhibitor (Thermo Scientific, USA.) and 10 µL of 100X phosphatase inhibitor (Thermo Scientific, USA.) were mixed in 970 µL of RIPA protein lysis buffer.